UNIVERSITY of HAWAI'I®
Ke Kulanui o Hawai'i

Wendy F. Hensel
President

DEPT. COMM. NO. 102

December 12, 2025

The Honorable Ronald D. Kouchi,
President and Members of the Senate
Thirty-Third State Legislature
Honolulu, Hawai'i 96813

The Honorable Nadine K. Nakamura, Speaker
and Members of the House of Representatives
Thirty-Third State Legislature
Honolulu, Hawai'i 96813

Dear President Kouchi, Speaker Nakamura, and Members of the Legislature:

For your information and consideration, the University of Hawai'i is transmitting a copy of the Report on Developing a Wildfire Forecasting System for Hawai'i (Act 200, Session Law of Hawai'i 2024) as requested by the Legislature.

In accordance with Section 93-16, Hawai'i Revised Statutes, this report may be viewed electronically at: https://www.hawaii.edu/govrel/docs/reports/2026/act200slh2024_2026_wildfire-forecast-system_report.pdf.

Should you have any questions about this report, please do not hesitate to contact Stephanie Kim at (808) 956-4250, or via e-mail at scskim@hawaii.edu.

Sincerely,

Wendy F. Hensel
President

Enclosure

2444 Dole Street, Bachman Hall
Honolulu, Hawai'i 96822
Telephone: (808) 956-8207
Fax: (808) 956-5286
An Equal Opportunity Institution

UNIVERSITY OF HAWAIʻI SYSTEM REPORT

REPORT TO THE 2026 LEGISLATURE

Report on Developing a Wildfire Forecasting System for Hawaiʻi

Act 200, SLH 2024

December 2025

Developing a Wildfire Forecasting System for Hawai‘i

Summary

Wildfires in Hawai‘i increasingly threaten both ecological integrity and human well-being, prompting an urgent demand for accurate forecasting systems to support mitigation and preparedness efforts. Extreme weather conditions, particularly short-term drought, have frequently coincided with wildfire occurrences in recent years, offering valuable context for wildfire probability forecasts. In Hawai‘i, where flammable invasive grasses fuel rapid fire spread, accurate forecasting is essential for protecting vulnerable ecosystems and communities. This study introduces a hybrid deep learning framework that integrates Convolutional Long Short-Term Memory (ConvLSTM) networks with attention mechanisms, optimized by the Firefly Algorithm, to forecast wildfire probabilities across Hawai‘i. The model uses an input sequence of wildfire probability maps from the previous four days (t, $t-1$, $t-2$, and $t-3$) and generates forecasts for the subsequent three days ($t+1$, $t+2$, and $t+3$). The model shows good agreement with observed wildfire events. For Honolulu County, the F1-scores are 0.7837, 0.7687, and 0.7651 for the 1-, 2-, and 3-day-ahead forecasts, respectively. For Hawai‘i County, the corresponding values are 0.8182, 0.7781, and 0.7749. The model performs satisfactorily for Maui County, with F1-scores of 0.8103, 0.7757, and 0.7785, and for Kaua‘i County, with F1-scores of 0.8387, 0.8101, and 0.7871. Validation against observed wildfire events demonstrates the model’s robustness in identifying fire-prone areas. This agreement is further supported by weekly drought classifications, which consistently shows that regions with higher predicted probability experience abnormally dry to moderate drought conditions. This connection indicates that the model responds well to short-term environmental stress that commonly precedes wildfire activity. Overall, this framework demonstrates a feasible potential for operational use in early warning systems, offering valuable insights for land managers, emergency responders, and policymakers in fire-prone regions. The wildfire forecasting system is available on the Hawai‘i Climate Data Portal (https://www.hawaii.edu/climate-data-portal/data-portal/).

Keywords: Fire probability forecasting, ConvLSTM-Attention model, Firefly algorithm optimization, Spatiotemporal modeling, Multi-day wildfire forecasting

Background

Wildfires, recognized as one of the most destructive natural disasters, pose significant threats to ecosystems, human settlements, and economies worldwide (Hamadeh et al., 2017; Hantson et al., 2015; Pilly Joseph Kagosi et al., 2020). Over the past two decades, wildfires have caused extensive ecological and economic damage, driven by climate change and human activities that disrupt natural ecosystems and alter fire cycles in diverse regions, including island environments (Mass and Ovens, 2024; Rezaie et al., 2023). According to Trauernicht et al. (2015), Hawai‘i’s annual burned area between 2005 and 2011 averaged 8,427 hectares (0.48% of its land area), which was higher than the proportion burned across the entire U.S. mainland (0.30%) and even exceeded the average of 12 fire-prone western states, including Alaska (0.46%).

Over recent decades, Hawai‘i has experienced almost a fourfold increase in the total area affected by wildland fires (Trauernicht, 2019). Although wildfires frequently ignite near developed landscapes, most of the burned area occurs in dry, nonnative grasslands and shrublands, which cover about 24% of the state (Trauernicht et al., 2015). These grass-dominated ecosystems, combined with invasive species, prolonged drought, and widespread land-use changes such as abandoned agricultural fields, create continuous and highly flammable fuel beds. As fires spread rapidly through these landscapes and advance toward forested watershed margins, they pose significant risks to native ecosystems, watershed integrity, and community safety. This escalating threat highlights the need for improved landscape-scale fire-risk assessment and stronger integration of pre-fire planning and prevention in land management strategies (Marris, 2023; Trauernicht, 2015; Trauernicht et al., 2015; Yelenik et al., 2024).

Several studies used historical fire records and long-term geo-environmental variables, including topography, land cover, vegetation indices, and climatic factors to generate wildfire susceptibility maps (Hai et al., 2023; Kalantar et al., 2020; Pandey et al., 2022). These maps provide the probability of wildfire occurrence over long periods and are therefore effective for identifying persistently high-risk areas over decadal scales. While wildfire susceptibility maps are valuable for long-term planning and mitigation, they are not suited for short-term early warning systems. To address this gap, Tran et al. (2025) developed hybrid Hunger Games Search (HGS)–Random Forest (RF) and Moth-Flame Optimization (MFO)–RF models to estimate high spatial-resolution (250 m × 250 m) near real-time daily wildfire probability for Hawai‘i. They used six conditioning factors (rainfall, maximum air temperature, relative humidity, normalized difference vegetation index, antecedent precipitation index, and land cover) as inputs to their models. The output remains limited to near real-time probability maps estimates rather than near-future forecasts, and therefore cannot describe how wildfire likelihood changes over the next several days. It is evident that neither the long-term susceptibility maps nor the RF-based near real-time probability estimates from Tran et al. (2025) address the operational needs that require 1–3 day wildfire forecasting for proactive planning, early warnings, and resource allocation. By supporting early detection and prevention, short-term wildfire forecasting can help reduce wildfire impacts and strengthen community resilience, making it an essential tool for mitigation and response strategies (McCaffrey, 2015; Thompson et al., 2019).

Efforts to adapt mainland fire-danger systems to Hawai‘i have been limited by the state’s sharp gradients in vegetation, climate, and topography, which differ substantially from the continental conditions for which models like National Fire Danger Rating System (NFDRS), FlamMap, and FARSITE were designed (Burgan et al., 1974; Fujioka et al., 2000; Weise et al., 2010). More advanced ignition models developed for the conterminous United States, including the RMRS 7-day ignition-forecasting system, rely on long-term ignition records, coarse 20-km reanalysis grids, and monthly statistical equations calibrated to mainland fire regimes (https://research.fs.usda.gov/firelab/products/dataandtools/real-time-forecasting-wildfire-ignitions-out-7-days). These characteristics make them unsuitable for Hawai‘i’s fast-drying grass fuels and highly localized microclimates. As a result, Hawai‘i continues to depend on Red Flag Warnings (http://www.prh.noaa.gov/hnl/pages/firewx.php) derived

from weather conditions at the Honolulu International Airport station, using thresholds for the Keetch-Bayram Drought Index, relative humidity, and wind speed (Chu, 1995; Chu et al., 2002; Dolling et al., 2009). As the Red Flag Warnings rely on weather data from a single station, they do not capture spatial variations in fire risk across the islands. Consequently, Red Flag Warnings may fail to be issued even under high-risk conditions elsewhere. For example, no Red Flags Warnings were issued during the large fires on Maui in 2019 and 2023. The absence of a spatially explicit system capable of capturing statewide changes in fire likelihood remains a critical operational gap and underscores the need for a forecasting framework tailored to Hawai‘i’s rapidly evolving fire environment.

The main objective of this study is to develop a near-future wildfire forecasting system for the State of Hawai‘i. This system is capable of forecasting wildfire probability 1-3 days ahead at a spatial resolution of 250 m. To the end, wildfire probability maps from the previous four days (generated by Tran et al. (2025)) are used as inputs to a hybrid deep learning framework that integrates Convolutional Long Short-Term Memory (ConvLSTM) networks with attention mechanisms, optimized by the Firefly Algorithm, to forecast wildfire probabilities across Hawai‘i. This study also addresses three research questions: (a) What are the benefits and limitations of applying deep learning models to short-term wildfire-probability forecasting? (b) How do attention-based methods improve the performance of wildfire-forecasting models? and (c) How does incorporating wildfire estimates from different number of previous days affect the performance of the wildfire forecasting model?

To the best of our knowledge, this is the first study that forecasts daily wildfire probability for Hawai‘i. This study contributes to the literature in several significant ways: 1) it develops a novel ConvLSTM-based deep learning framework that generates short-term (1–3 day) wildfire-probability forecasts, 2) it incorporates an attention mechanism to strengthen temporal learning and improve forecast accuracy, 3) it evaluates the fire forecasts against weekly drought conditions, 4) it applies the Firefly Algorithm to optimize ConvLSTM hyperparameters, thereby improving forecasting accuracy, 5) it compares the wildfire forecasts with the historical wildfire maps from Tran et al. (2025); and finally 6) it compares the wildfire forecasts with reported wildfire events. The wildfire forecasting system from this study offers a valuable tool for land-use planners, emergency responders, and policymakers to mitigate wildfire impacts on Hawai‘i's communities and ecosystems.

Data and preprocessing

Study area

The study area covers the State of Hawai‘i, which is comprised of four counties (i.e., seven islands): Honolulu, Maui, Kaua‘i, and Hawai‘i counties (Figure 1). The State of Hawai‘i encompasses a land area of 16,635 km^2 with a resident population of 1.4 million. Wildfire locations from 2002-2020 are indicated in Figure 1 with circles.

Hawai‘i's climate is primarily shaped by orographic precipitation, where moist northeasterly trade winds bring significant precipitation to the windward sides of the

islands' volcanic mountains, resulting in drier conditions on the leeward side (Giambelluca et al., 2013). Mean annual precipitation varies widely, ranging from 264 mm to over 6400 mm (Tran et al., 2024), with a rainy season from November to April and a dry season from May to October (Frazier and Giambelluca, 2017). Hawai‘i’s average annual temperatures range modestly between 9°C and 23.8°C, but have shown a notable upward trend since the mid-1970s, in line with the global warming trend (Giambelluca et al., 2008). This temperature rise has led to changes in evapotranspiration and precipitation levels. Relative humidity also varies across the islands, with annual averages between 60% and 86% (Tran et al., 2024). Under trade wind conditions, a distinct moisture transition occurs between 1200 and 2400 m; below these elevations, the air is moist, while above, it becomes dry. This difference is due to a temperature inversion within the moving trade wind air (Blumenstock and Price, 1974).

Normalized Difference Vegetation Index (NDVI) is a widely used remote sensing index for evaluating vegetation density and overall ecosystem condition. Tran et al. (2025) reported that mean annual NDVI values across Hawai‘i range from –0.2 to 0.8. Long-term analyses by Madson et al. (2023) further show that NDVI has declined substantially across the Hawaiian Islands between 1982 and 2019, with the most pronounced reductions (≥44%) occurring on Lāna‘i and Hawai‘i Island.

Hawai‘i’s landscapes are incredibly diverse, with land cover types ranging from lowland shrublands to high-elevation alpine areas. In recent years, changes in land use have been driven by the decline of agriculture (Perroy et al., 2016), the growth of commercial forestry (Ares and Fownes, 2000) and increasing housing development.

Tran et al. (2025) shows the distribution of three main types of vegetation/covers across the state. Woody or coarse vegetation includes green dense woody vegetation that is over 5 meters high. Grass cover refers to low-growing fine vegetation and green or dry nonwoody herbaceous plants such as forbs, ferns, and graminoids. Bare earth includes all areas without vegetation and encompasses a wide variety of soil series and ages found across Hawai‘i, ranging from young bare lava flows to aged weathered oxisoils and andisols (Lucas, 2017).

Observational records indicate a rapid increase in air temperature across Hawai‘i over the past four decades (Giambelluca et al., 2008; Longman et al., 2019). As the state continues to warm, wildfire frequency and total burned area have also increased and are projected to rise further (Tran et al. 2025). This escalation in fire activity is driven largely by the abandonment of agricultural lands, which has facilitated the expansion of fire-prone invasive grasslands and shrublands that now occupy approximately 25% of Hawai‘i’s land area (~800,000 hectares), coupled with declining resources and institutional support historically available for firefighting (Trauernicht et al., 2015). Recent outcomes of these landscape and climate changes include more than 17,000 acres burned on Maui in 2019, the 2018 West O‘ahu fire complex (~4,500 acres), the West Maui fires during Hurricane Lane in 2018—burning 23 homes and forcing evacuations—and the 2023 Maui wildfires, which caused over 100 fatalities and destroyed or damaged roughly 3,000 structures, marking the deadliest U.S. wildfire in more than a century.

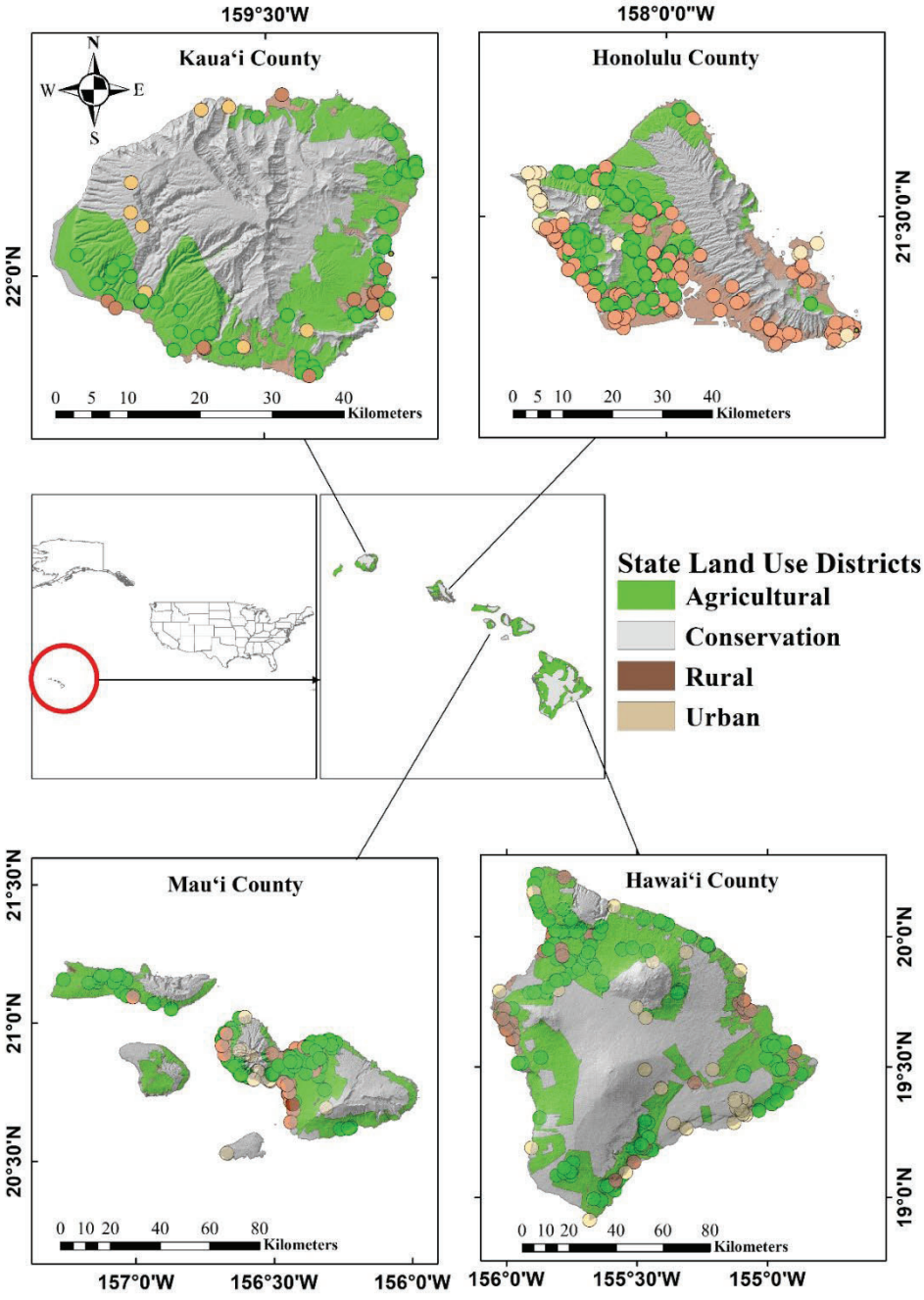

Figure 1. The selected study areas and recorded wildfire occurrences from 2002 to 2020.

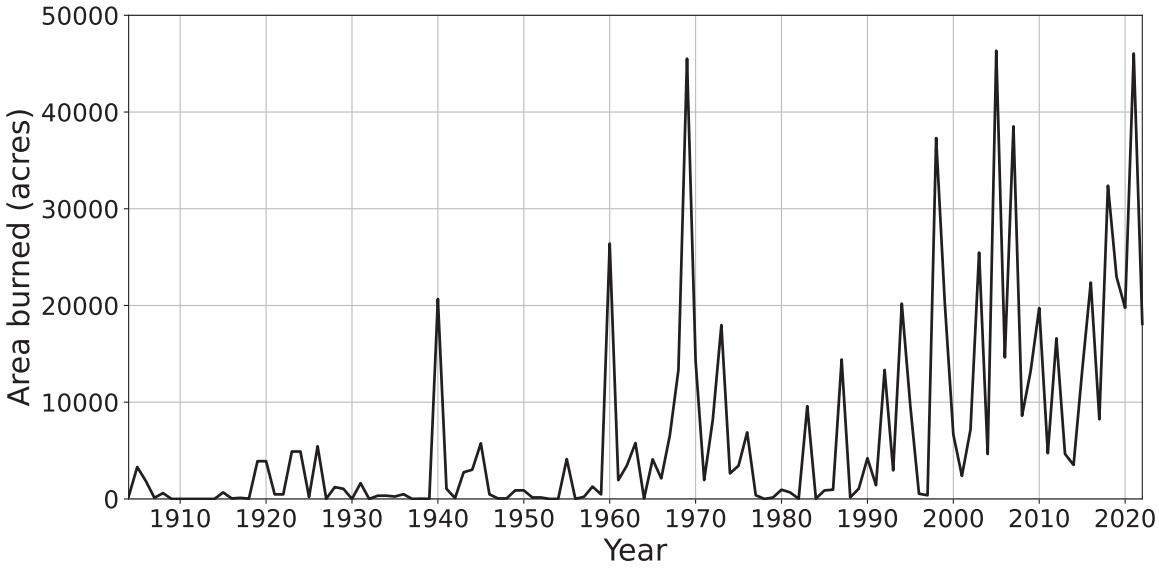

Figure 2. Annual area burned in the State of Hawai'i for 1904-2022.

Data description

In this study, we utilized historical daily wildfire probability estimates from Tran et al. (2025). We incorporated these probabilities as input variables into developed models to forecast fire probability 1, 2, and 3 days ahead (i.e., *t*+1, *t*+2, and *t*+3), where *t* represents the current day. To determine the optimal input configuration (i.e., number of lags) for accurate forecasting, we systematically tested three different configurations: a 2-day lag (*t*, *t*-1), a 3-day lag (*t*, *t*-1, *t*-2), and a 4-day lag (*t*, *t*-1, *t*-2, *t*-3). These lags represent the days preceding the first forecast day (*t*+1), during which wildfire probability estimates from Tran et al. (2025) were incorporated into developed models as predictive variables. This approach enabled us to examine how different input lag lengths influence predictive performance, ensuring that the model effectively captures the temporal evolution of wildfire risk while reducing the potential for overfitting. By adjusting the input structure, we aimed to enhance the model's ability to learn from historical patterns and improve its forecasting accuracy.

The wildfire probability forecasts from this study are evaluated against observed wildfire occurrences in Hawai'i. Wildfire records were obtained from the Honolulu Fire Department, the Division of Forestry and Wildlife (DOFAW), Hawai'i Wildfire Management Organization (HWMO), and Hawai'i Volcanoes National Park (HVNP) for all four counties, covering the period from January 1, 2002, to December 31, 2020. These records were used for model validation, providing the ground-truth observations needed to assess forecast performance through sensitivity, specificity, negative predictive value (NPV), positive predictive value (PPV), the F1-score (the harmonic mean of sensitivity and precision), and the area under the ROC curve (AUC) metrics. These wildfire records contain comprehensive data on each incident, such as geographic location, burned area, and the date of occurrence. To be consistent with Tran et al. (2025) and to ensure the analysis concentrated on major wildfire events, only fire surpassing 8 acres in size were

included. Consequently, the dataset comprises 292 fire events in Honolulu County, 188 in Hawai‘i County, 90 in Maui County, and 78 in Kaua‘i County between 2002 and 2020.

Drought Condition

Weekly drought classification data were obtained from the U.S. Drought Monitor (https://droughtmonitor.unl.edu/CurrentMap.aspx), a collaborative product of the University of Nebraska–Lincoln, USDA, and NOAA. The dataset provides spatially explicit drought severity levels across the United States on a weekly basis, categorized into five main drought intensity levels: D0 (Abnormally Dry), indicating short-term dryness that may precede or follow drought; D1 (Moderate Drought), involving some damage to crops and pastures with developing water shortages; D2 (Severe Drought), reflecting likely crop or pasture losses and the need for water restrictions; D3 (Extreme Drought), denoting major agricultural losses and widespread water shortages; and D4 (Exceptional Drought), representing severe, prolonged drought impacts that often require emergency responses (Noel et al., 2020).

As daily drought records are unavailable, weekly data were utilized to identify the nearest drought condition corresponding to forecasted fire-prone days. To classify drought severity levels in this study, we adopted the drought categorization system based on the Standard Precipitation Index (SPI) and Standardized Precipitation-Evapotranspiration Index (SPEI), as summarized in Table 1. Each drought category was assigned a specific color for mapping purposes to enhance visual interpretation.

Table 1. Drought severity categories based on SPI and SPEI values and associated percentile ranges, color-coded for map visualization.

Category	Description	Example Percentile Range	SPI/SPEI Values Range
None	Normal or wet conditions	30.01 or above	-0.49 or above
D0	Abnormally Dry	20.01 to 30.00	-0.5 to -0.79
D1	Moderate Drought	10.01 to 20.00	-0.8 to -1.29
D2	Severe Drought	5.01 to 10.00	-1.3 to -1.59
D3	Extreme Drought	2.01 to 5.00	-1.6 to -1.99
D4	Exceptional Drought	0.00 to 2.00	-2.0 or less

Methodology

ConvLSTM network

ConvLSTM, a variant of the traditional LSTM (Long Short-Term Memory) network, incorporates convolutional operations into the standard LSTM architecture to effectively capture both temporal and spatial dependencies in time series data (Shi et al., 2015). This capability is particularly advantageous for wildfire forecasting, where both spatial

patterns (e.g., topography, land cover type) and temporal sequences (e.g., weather data, vegetation conditions) play a critical role in fire occurrences.

The core advantage of the ConvLSTM model lies in its ability to utilize memory cells for input, forget, and output gates through convolutional operations rather than fully connected layers, as in traditional LSTM networks (Moishin et al., 2021; Shi et al., 2015). This allows the model to retain spatial information from multidimensional input data, such as gridded weather datasets and vegetation indices, ensuring that relevant spatial features are not lost during the forecasting process.

The ConvLSTM model handles the following gates through convolutional operations:

Forget Gate (f_f): Determines the amount of information from the previous time step's memory cell to be discarded.

Input Gate (i_i): Controls how much new information from the current input will be added to the memory cell.

Cell State Update (C_t): Updates the memory cell state by combining the retained information from the forget gate and the new information from the input gate.

Output Gate (o_t): Determines how much of the updated cell state will be used to generate the current output.

The equations governing these gates are given as follows (Shi et al., 2015):

$$f_f = \sigma(W_f * X_t + U_f * h_{t-1} + V_f * C_{t-1} + b_f) \quad (1)$$

$$i_t = \sigma(W_i * X_t + U_i * h_{t-1} + V_i * C_{t-1} + b_i) \quad (2)$$

$$C_t = f_t \times C_{t-1} + i_t \times \tanh(W_c * X_t + U_c * h_{t-1} + b_c) \quad (3)$$

$$o_t = \sigma(W_o * X_t + U_o * h_{t-1} + V_o * C_{t-1} + b_o) \quad (4)$$

$$h_t = o_t \times \tanh(C_t) \quad (5)$$

where * denotes convolution and × the Hadamard product; X_t and h_t represent the input and hidden state at time *t* (with *t*−1 indicating the previous step); W_f, W_i, W_c, W_o and U_f, U_i, U_c, U_o are the convolutional kernels for input-to-state and hidden-to-state transitions; V_f, V_i, V_c, V_o are peephole connections from the cell state; and σ denotes the sigmoid activation function.

A key difference between ConvLSTM and traditional LSTM is the use of peephole connections, where all gates have access to the previous memory cell content (C_{t-1}), even when the output gate is closed. This peephole connection ensures that the impact of earlier inputs is preserved across long input sequences, which is crucial for accurately capturing wildfire dynamics over time (Rahman and Siddiqui, 2019).

ConvLSTM-Attention model

In 2014, a team from Google innovatively integrated the attention mechanism into a deep learning recurrent neural network, yielding significant advancements in image classification tasks (Mnih et al., 2014). This pioneering application marked the beginning of widespread adoption of the attention mechanism in scholarly research across various fields. Bahdanau et al. (2015) successfully applied the attention mechanism to natural language processing, significantly enhancing translation algorithms. In 2017, Google's research team introduced the Transformer encoder-decoder algorithm (Vaswani et al., 2017), which exclusively utilized the self-attention mechanism. This approach departed from the traditional recurrent and convolutional neural networks commonly employed in deep learning. By leveraging the fundamental attributes of neural networks, the transformer demonstrated exceptional performance across various natural language processing tasks.

The attention mechanism is inspired by human visual attention, where the visual system does not uniformly process an entire scene. Instead, it selectively focuses on specific areas of interest within the scene. In essence, when an algorithm identifies that certain information within a scene consistently correlates with the label, it learns to prioritize this information in similar future scenarios, enhancing efficiency by focusing less on other areas. This principle that underpins the ConvLSTM-Attention network structure is depicted in Figure 3.

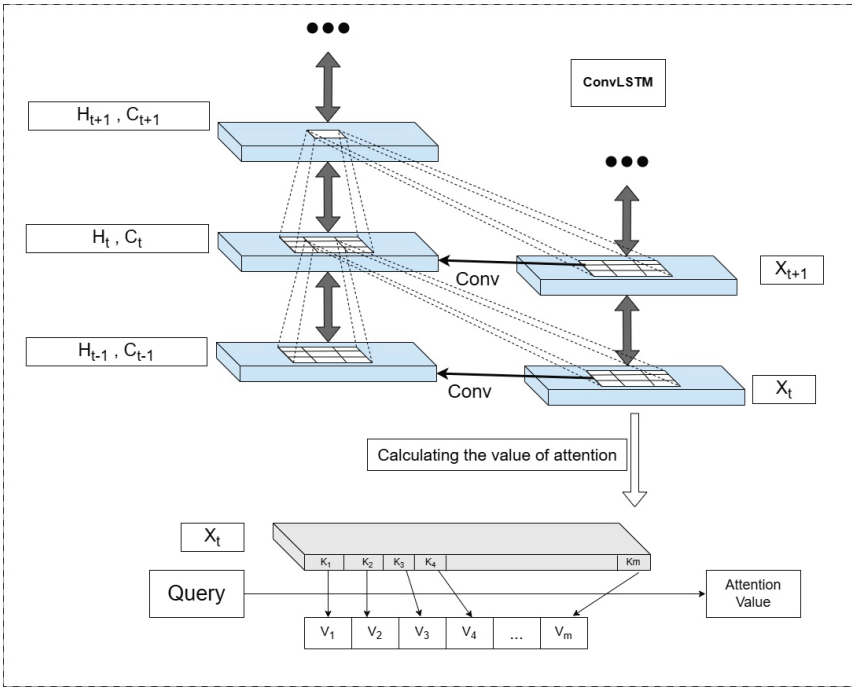

Figure 3. Schematic of a ConvLSTM-Attention model.

In the ConvLSTM–Attention architecture, the Query (Q) represents the feature vector at the current time step, while the Keys (K_1, …, K_m) and Values (V_1, …, V_m) correspond to spatial–temporal feature representations extracted from earlier ConvLSTM hidden states

or from patches of the input sequence. The attention computation follows three main steps: (1) the model first computes a similarity score between the query Q and each key K_m, typically using dot-product or additive attention (Bahdanau et al., 2015); (2) these similarity scores are then normalized through a softmax function to produce attention weights that sum to one; and (3) the normalized weights are applied to the corresponding value vectors V_m, and a weighted summation is performed to obtain the final attention output. In this formulation, each V_m represents the value vector associated with key K_m, capturing encoded spatial–temporal information that the model selectively re-weights and integrates to emphasize the most relevant regions or time steps for prediction.

The fundamental component of the attention mechanism involves a set of weight parameters. These parameters are iteratively adjusted to learn the association strength between each element in the sequence and the corresponding label. Based on this learned correlation, the attention module then reallocates weights to the original inputs, effectively reassigning importance to different parts of the input data. The attention module is responsible for assigning weight parameters. By integrating this module, different vectors in a sequence are allocated varying levels of attention, which reflects their respective impacts on predicting current information. This inclusion of new information significantly enhances the efficiency of network learning.

Firefly algorithm

The firefly algorithm (FA) is one of the most prominent swarm-based metaheuristic algorithm, which was introduced by Yang (2009). It is built based on three rules: 1) fireflies are attracted to each other regardless of gender; 2) attractiveness of fireflies is proportional to their brightness, meaning that less bright fireflies move toward brighter ones; and 3) the brightness is determined by evaluating the fitness function (Larabi Marie-Sainte and Alalyani, 2020). The FA divides the population into subgroups during the iterative optimization process, with each subgroup located near a local extremum in the search space. This division facilitates the search for the global optimal solution and makes the FA capable of solving non-linear and multi-model optimization problems (Nayak et al., 2020). During the iterative optimization process, certain parameters of the FA can be adjusted dynamically based on the optimization conditions, which can accelerate the algorithm's convergence speed. In the FA, every firefly is drawn towards any firefly brighter than itself, which leads to a high convergence performance (Li et al., 2022). The FA does not require a good initial solution and always results in the same optimal solution regardless of the starting point. The readers are referred to Fister et al. (2013) for a detailed description of the FA and its mathematical expressions.

Model assessment

The evaluation of wildfire forecasts from the developed models are conducted through a two-step process. First, the forecasted wildfire probability maps for 1, 2, and 3 days ahead were compared with the existing wildfire risk maps from Tran et al. (2025). This comparative analysis utilized several statistical metrics widely used in predictive modeling and error measurement. The coefficient of determination (R^2) indicates the proportion of variance in the reference data that is explained by the forecasts. Higher R^2 values reflect better agreement between the wildfire probability forecasts from this study and the historical estimates from Tran et al. (2025). Root Mean Squared Error (RMSE) provides

a direct measure of the average forecasting error relative to the historical estimates. Mean Squared Error (MSE) represents the average of the squared differences between the forecasts (this study) and the historical estimates from Tran et al. (2025). Mean Absolute Error (MAE) shows the average of the absolute differences between the forecasts and historical estimates.

Following this initial validation, the wildfire forecasts underwent a further assessment using historical wildfire events records from 2002 to 2020 to validate their robustness in real-world scenarios. This phase focused on classification accuracy, utilizing metrics such as Precision (Positive Predictive Value) and NPV to evaluate the model's capability to correctly classify wildfire and non-wildfire events (Umberger et al., 2017). Recall (Sensitivity) and Specificity were computed to determine the model's efficiency in identifying both wildfires and non-wildfires events (Naidu et al., 2023). The AUC was employed to assess the model's performance across various threshold levels, which is important for applications in environments with imbalanced datasets (Hand, 2009). Additionally, the F1 Score was calculated to provide a balanced measure of the model's precision and recall, offering a single metric that summarizes the model's overall accuracy in detecting wildfires (Wardhani et al., 2019). The equations for Sensitivity, Specificity, PPV, NPV, and F1 Score are given by,

$$Sensitivity = \frac{TP}{TP + FN} \tag{6}$$

$$Specificity = \frac{TN}{FP + TN} \tag{7}$$

$$PPV = \frac{TP}{TP + FP} \tag{8}$$

$$NPV = \frac{TN}{FN + TN} \tag{9}$$

$$F1\ score = 2 \times \frac{PPV \times Sencitivity}{PPV + Sencitivity} \tag{10}$$

where TP (true positive) represents the number of correctly identified wildfire pixels, TN (true negative) denotes the number of correctly classified non-wildfire pixels, FP (false positives) shows the number of non-wildfire pixels misclassified as wildfires, and FN (false negatives) indicates the number of wildfire pixels incorrectly classified as non-wildfires.

Through these comprehensive assessment phases, our study not only compares the wildfire forecast maps against historical estimates from Tran et al. (2025), but also evaluate them using historical wildfire records, ensuring their value for wildfire management and response strategies.

Results

Model tuning

To improve the performance of the ConvLSTM and ConvLSTM-Attention models, we applied the Firefly Algorithm to systematically search for the optimal hyperparameter

configurations. This approach enabled efficient tuning by exploring a wide range of possible hyperparameter values while avoiding local optima, ensuring improved model convergence and predictive accuracy. Table 2 summarizes the optimized hyperparameters obtained by the Firefly Algorithm. The tuning process focused on selecting the optimal number of filters, kernel sizes, activation functions, and batch normalization settings, as well as determining the most effective learning rate for the Adam optimizer. The Firefly Algorithm identified a set of hyperparameters that minimized the mean squared error (MSE) and improved the classification performance, particularly the F1-score.

A key observation from the tuning process was that the ConvLSTM-Attention model required fewer filters than the standard ConvLSTM model, as the attention mechanism effectively prioritized critical spatial-temporal features, reducing the need for additional feature-extraction layers. Additionally, the Firefly Algorithm identified that a kernel size of 3×3 in the ConvLSTM layers provided the best balance between computational efficiency and predictive accuracy. By using the Firefly Algorithm for hyperparameter selection, we achieved improved model generalization and faster convergence, ensuring the robustness of wildfire probability forecasting across the State of Hawai‘i. The detailed hyperparameter settings and optimization results are provided in Table 2.

Table 2. Optimized hyperparameters for the ConvLSTM-Attention model.

Hyperparameter	Value	Description
Number of ConvLSTM Layers	2	Two stacked ConvLSTM layers for spatiotemporal encoding
Filters (Layers 1 & 2)	128, 64	Number of filters in first and second ConvLSTM layers
Kernel Size (ConvLSTM)	3×3	Size of the convolutional kernel
Activation Function	Tanh (ConvLSTM), Sigmoid (Final), Softmax (Attention)	Nonlinearities applied in different model components
Return Sequences	TRUE (L1), FALSE (L2)	Whether to return full sequences or final outputs
Attention Mechanism	Multi-head	Spatial-channel attention applied between layers
Attention Kernel Size	(1×1×1)	Kernel size for attention computation

Batch Normalization	Applied (after each layer)	Stabilizes training and improves generalization
Optimizer	Adam	Adaptive moment estimation for training
Learning Rate	0.001	Initial learning rate for the optimizer
Loss Function	Mean Squared Error (MSE)	Measures difference between predicted and true values
Output Channels	3	Number of output channels for multi-day forecast
Input Sequence Length	4 days	Number of previous days used as input

Evaluation of Forecasted Wildfire Maps

In this study, wildfire probability maps were forecasted for Honolulu, Maui, Hawai‘i, and Kaua‘i counties using the ConvLSTM and ConvLSTM-Attention models. To evaluate the impact of temporal dependencies on predictive performance, we applied three different lag configurations: 2-, 3-, and 4-day lags. These configurations allowed for a comparative assessment of how varying lag lengths influence the accuracy of wildfire risk forecasting. These forecasts illustrate the model's ability to identify high-risk areas across different time horizons and to simulate the spatial and temporal evolution of wildfire risk. The following subsections provide a detailed analysis of wildfire risk forecasting for each county, highlighting key fire-prone regions and evaluating the model's ability to detect fire occurrences.

Honolulu County

The forecasted wildfire maps for 1, 2, and 3 days ahead are compared with the historical wildfire probability maps from Tran et al. (2025) for Honolulu County, using 2-, 3-, and 4-day lags (Table 3). The results for the 3- and 4-day lags are very close and better than the 2-day lag configuration. Both the ConvLSTM and ConvLSTM-Attention models achieved high R^2 values, and low RMSE and MAE across all forecast horizons. The ConvLSTM model reached R^2 values between 0.9462 and 0.9629, with RMSE ranging from 0.0374 to 0.0452, and MAE from 0.0169 to 0.0212. These values show strong spatial agreement between the 1- to 3-day forecasts and the historical wildfire probability maps from Tran et al. (2025). The ConvLSTM-Attention model obtained R^2, RMSE, and MAE values that were very close to those of the ConvLSTM model, with RMSE and MAE improving by about 3% to 5% in several configurations. This suggests that the attention mechanism enhances the model's sensitivity to changes in wildfire probability by re-weighting the most informative features. Overall, these results indicate that the forecasts for Honolulu County aligned well with the historical wildfire probability patterns across the 1- to 3-day lead times.

The spatial comparisons for March 29, March 30, and April 4, 2021 are shown in Figures 4, 5, and 6, respectively, with the forecasted wildfire probability maps in the top row, the Tran et al. (2025) maps in the middle row, and the absolute misfit in the bottom row.

These figures show strong agreement between our forecasts and the historical wildfire probability maps across the 1-, 2-, and 3-day lead times. Tran et al. (2025) identified higher wildfire probabilities in the south, west, southeast, and northwest of Honolulu County during these dates, and these patterns are consistently captured in our forecasts. Probabilities close to 0 and 1 indicate low and high wildfire likelihoods, respectively. In the 1-day-ahead forecast (Figure 4), misfit values remain very low across the county, generally below 0.05. The 2-day-ahead forecast (Figure 5) shows a modest increase in misfit in parts of the western region, and the 3-day-ahead forecast (Figure 6) displays the largest differences. Even with these increases, most misfit values remain below 0.1 across Honolulu County. These spatial results agree with the numerical metrics, with RMSE values across the three selected dates ranging from 0.033 to 0.042 for the 1-day forecasts, 0.050 to 0.062 for the 2-day forecasts, and 0.057 to 0.075 for the 3-day forecasts.

Table 3. Comparison of forecasted wildfire probability maps for 1-, 2-, and 3-day-ahead with the historical wildfire probability maps from Tran et al. (2025) for Honolulu County.

County	Model	Configuration	R^2			RMSE			MAE		
			1 day	2 days	3 days	1 day	2 days	3 days	1 day	2 days	3 days
Honolulu	ConvLSTM	2-day-lag	0.9586	0.9491	0.9462	0.0395	0.0439	0.0452	0.0183	0.0208	0.0212
		3-day-lag	0.9628	0.9555	0.9548	0.0374	0.0411	0.0414	0.0187	0.0204	0.0207
		4-day-lag	0.9629	0.9537	0.9529	0.0374	0.0419	0.0423	0.0169	0.0193	0.0193
	ConvLSTM-Attention	2-day-lag	0.9611	0.9561	0.9544	0.0381	0.0408	0.0415	0.0171	0.0189	0.0192
		3-day-lag	0.9630	0.9578	0.9562	0.0372	0.0399	0.0405	0.0168	0.0184	0.0187
		4-day-lag	0.9624	0.9573	0.9557	0.0376	0.0402	0.0410	0.0179	0.0193	0.0196

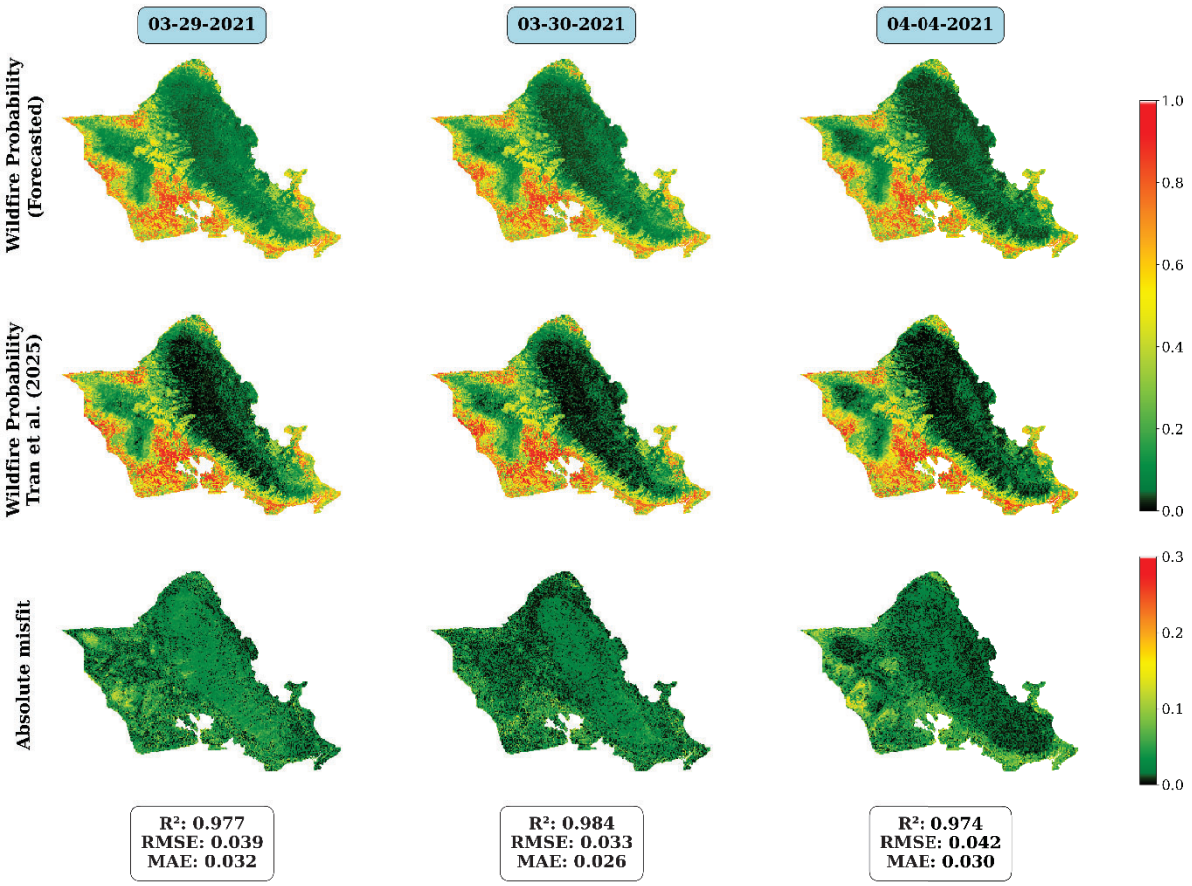

Figure 4. (Top row) 1-day-ahead forecasted wildfire probability maps, (middle row) historical wildfire probability estimates from Tran et al. (2025), and (bottom row) the absolute misfit between the top and middle rows for three sample days in Honolulu County.

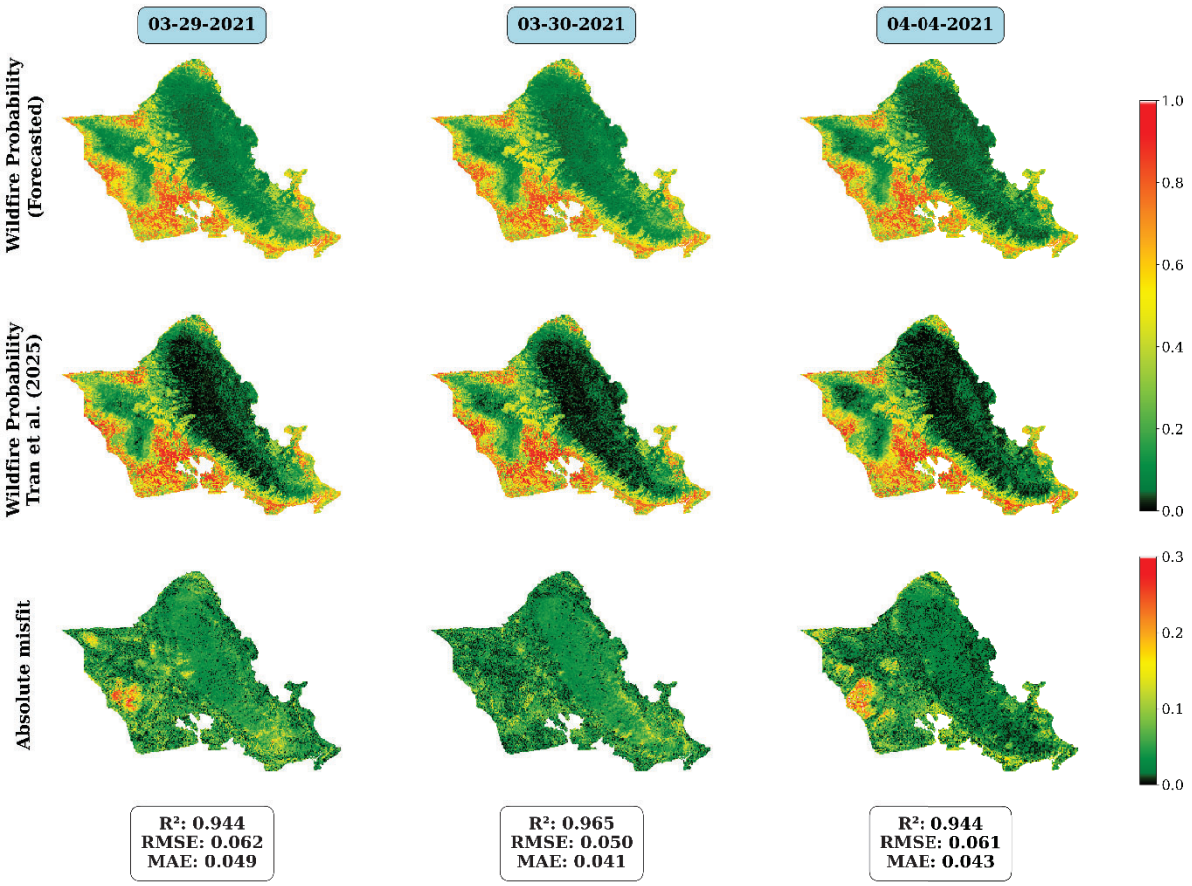

Figure 5. (Top row) 2-day-ahead forecasted wildfire probability maps, (middle row) historical wildfire probability estimates from Tran et al. (2025), and (bottom row) the absolute misfit between the top and middle rows for three sample days in Honolulu County.

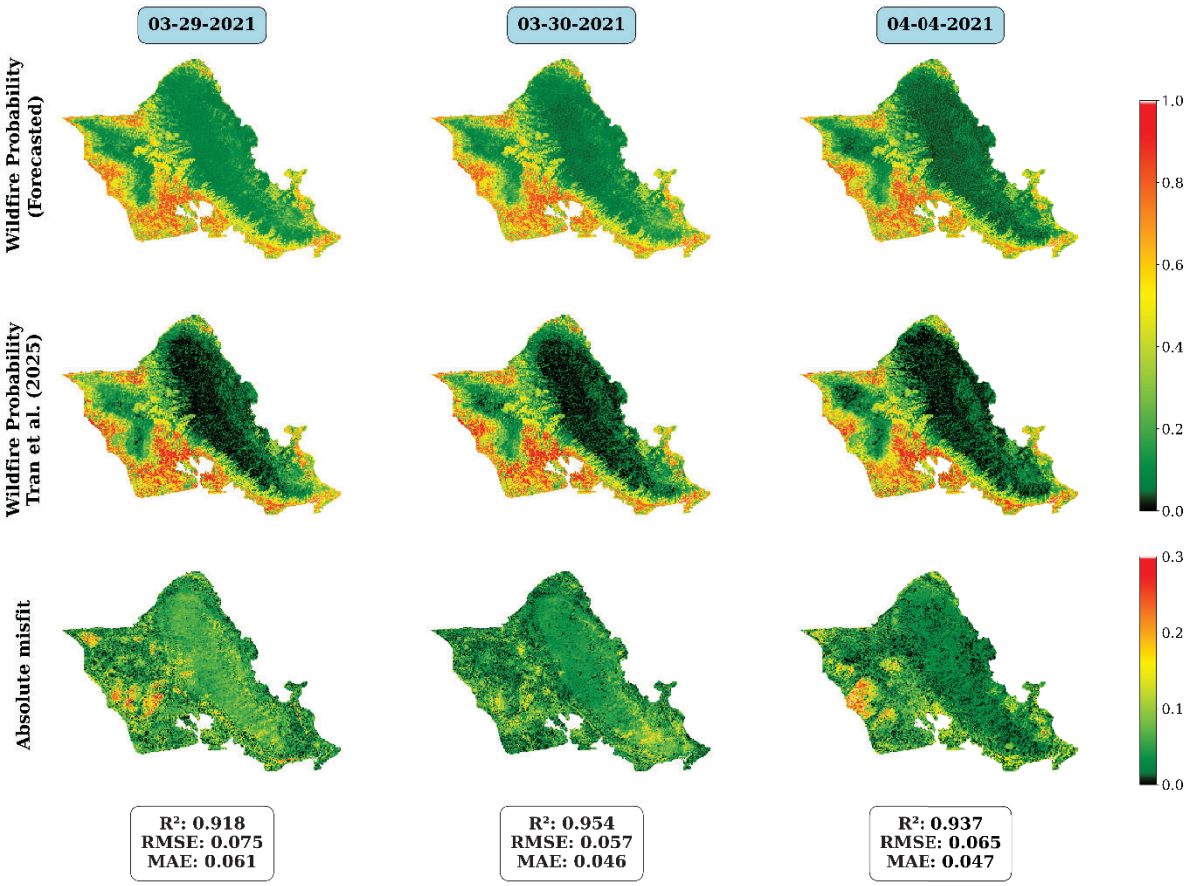

Figure 6. (Top row) 3-day-ahead forecasted wildfire probability maps, (middle row) historical wildfire probability estimates from Tran et al. (2025), and (bottom row) the absolute misfit between the top and middle rows for three sample days in Honolulu County.

Moreover, the performance of the ConvLSTM and ConvLSTM-Attention models is evaluated against historical wildfire records (Table 4). The ConvLSTM model shows consistent performance across the three forecast horizons. For the 1-day forecasts, sensitivity ranges from 0.7103 to 0.7345, specificity from 0.8138 to 0.8241, NPV from 0.7399 to 0.7532, PPV from 0.7948 to 0.8016, F1-scores from 0.7532 to 0.7634, and AUC values from 0.8250 to 0.8288. For the 2-day forecasts, sensitivity ranges from 0.7138 to 0.7345, specificity from 0.8103 to 0.8138, NPV from 0.7398 to 0.7540, PPV from 0.7931 to 0.7978, F1-scores from 0.7514 to 0.7648, and AUC from 0.8209 to 0.8282. For the 3-day forecasts, sensitivity ranges from 0.6662 to 0.7276, specificity from 0.8138 to 0.8207, NPV from 0.7217 to 0.7492, PPV from 0.7766 to 0.7992, F1-scores from 0.7330 to 0.7604, and AUC from 0.8195 to 0.8273.

Among the two models, the ConvLSTM-Attention model with a 4-day input lag demonstrates the closest correspondence with the observed wildfire records. For the 1-day-ahead forecasts, this configuration yields high scores across all metrics (sensitivity = 0.7310, specificity = 0.8655, NPV = 0.7629, PPV = 0.8446, F1-score = 0.7837, and AUC = 0.8544), including the highest PPV and AUC among all configurations. For the 2- and

3-day-ahead forecasts, the 4-day-lag ConvLSTM-Attention model attains the highest sensitivity (0.7448 and 0.7414), NPV (0.7597 and 0.7565), F1-scores (0.7687 and 0.7651), and AUC values (0.8302 and 0.8304), demonstrating stronger predictive performance at the longer forecast horizons compared with the other models. Using the 4-day input lag, the ConvLSTM-Attention model shows consistent overall improvement when compared with the ConvLSTM model across most evaluation metrics. Although individual lead times show minor reductions in specificity and PPV, the average change across the 1-, 2-, and 3-day forecasts indicates increases of 2.58% in sensitivity, 1.29% in specificity, 2.00% in NPV, 1.76% in PPV, 2.14% in F1-score, and 1.31% in AUC. These gains indicate that the 4-day-lag ConvLSTM-Attention configuration provides the most accurate wildfire detection for Honolulu County.

Table 4. Comparison of forecasted wildfire probability maps for 1-, 2-, and 3-day-ahead with the wildfire records for Honolulu County.

Metric indices	Lead time (day)	ConvLSTM			ConvLSTM-Attention		
		2-day-lag	3-day-lag	4-day-lag	2-day-lag	3-day-lag	4-day-lag
Sensitivity	1	0.7103	0.7276	0.7345	0.7000	0.7448	0.7310
	2	0.7310	0.7345	0.7138	0.7034	0.7345	0.7448
	3	0.6662	0.7276	0.7138	0.7034	0.7310	0.7414
Specificity	1	0.8241	0.8138	0.8103	0.8690	0.8483	0.8655
	2	0.8103	0.8138	0.8138	0.8172	0.8172	0.8069
	3	0.8138	0.8138	0.8207	0.8172	0.8138	0.8034
NPV	1	0.7399	0.7492	0.7532	0.7434	0.7688	0.7629
	2	0.7508	0.7540	0.7398	0.7337	0.7548	0.7597
	3	0.7217	0.7492	0.7414	0.7337	0.7516	0.7565
PPV	1	0.8016	0.7962	0.7948	0.8423	0.8308	0.8446
	2	0.7940	0.7978	0.7931	0.7938	0.8008	0.7941
	3	0.7766	0.7962	0.7992	0.7938	0.7970	0.7904
F1-score	1	0.7532	0.7604	0.7634	0.7646	0.7855	0.7837
	2	0.7612	0.7648	0.7514	0.7459	0.7662	0.7687
	3	0.7330	0.7604	0.7541	0.7459	0.7626	0.7651
AUC	1	0.8250	0.8288	0.8284	0.8500	0.8519	0.8544

	2	0.8209	0.8282	0.8268	0.8260	0.8276	0.8302
	3	0.8195	0.8273	0.8272	0.8260	0.8284	0.8304

Maui County

The forecasted wildfire probability maps for 1, 2, and 3 days ahead are compared with the historical wildfire probability maps from Tran et al. (2025) for Maui County in Table 5. The ConvLSTM and ConvLSTM-Attention models show almost identical performance for the 1- and 2-day forecasts, with both models reaching R^2 values above ~0.95 and RMSE values around 0.04–0.05. For the 3-day forecasts, the ConvLSTM-Attention model with the 4-day-lag configuration performs best, reducing RMSE by approximately 10% compared to the corresponding ConvLSTM configuration (0.0454 vs. 0.0503). Based on this improvement, the ConvLSTM-Attention model with 4-day-lag was selected as the preferred model. Overall, the models maintain good agreement with the historical wildfire probability maps from Tran et al. (2025).

The spatial comparisons for March 27, April 1, April 4, and April 30, 2021 are shown in Figures 7, 8, and 9, with the ConvLSTM-Attention forecasted wildfire probability maps in the top row, the Tran et al. (2025) maps in the middle row, and the absolute misfit in the bottom row. These figures illustrate the close agreement between the wildfire probability forecasts and historical wildfire probability estimates across Maui County. Tran et al. (2025) indicated higher wildfire probability across the central valley and the leeward regions of Maui Island, as well as in several areas on Lānaʻi, Molokaʻi, and Kahoʻolawe, and these spatial patterns are captured fairly well in the forecasts. For the 1-day-ahead forecasts (Figure 7), three of the four dates show strong agreement, with R^2 values between 0.919 and 0.968 and RMSE values between 0.044 and 0.062, while the April 1 case exhibits weaker performance (R^2 = 0.830, RMSE = 0.090), reflecting noticeable mismatches on Molokaʻi and Kahoʻolawe. The 2-day-ahead forecasts (Figure 8) show a similar pattern: March 27, April 4 (in most areas), and April 30 align well with the historical maps (R^2 between 0.692 and 0.896; RMSE between 0.083 and 0.120), but the April 1 forecast shows substantially lower agreement (R^2 = 0.343; RMSE = 0.177). The 3-day-ahead forecasts (Figure 9) remain consistent on March 27, April 4, and April 30 (R^2 between 0.617 and 0.834; RMSE between 0.094 and 0.134), while showing a weak agreement on April 1 (R^2 = 0.288; RMSE = 0.184). Aside from April 1, the misfit values are mostly below 0.15, indicating small spatial differences between the forecasted and historical probability maps. Despite the weak performance on April 1, the forecasts for the other three dates maintain low misfit values and reproduce the main wildfire-prone areas identified by Tran et al. (2025). RMSEs across the four selected dates range from 0.044 to 0.090 for the 1-day forecasts, 0.080 to 0.177 for the 2-day forecasts, and 0.094 to 0.184 for the 3-day forecasts. Despite the weak performance on April 1, the forecasts for the other three dates maintain low misfit values and reproduce the main wildfire-prone areas identified by Tran et al. (2025).

Table 5. Comparison of forecasted wildfire probability maps for 1-, 2-, and 3-day-ahead with the historical wildfire probability maps from Tran et al. (2025) for Maui County.

County	Model	Configuration	R^2			RMSE			MAE		
			1 day	2 days	3 days	1 day	2 days	3 days	1 day	2 days	3 days
Maui	ConvLSTM	2-day-lag	0.9574	0.9519	0.9496	0.0434	0.0461	0.0472	0.0170	0.0179	0.0178
		3-day-lag	0.9625	0.9568	0.9530	0.0408	0.0437	0.0456	0.0166	0.0176	0.0184
		4-day-lag	0.9603	0.9496	0.9428	0.0419	0.0472	0.0503	0.0149	0.0170	0.0183
	ConvLSTM-Attention	2-day-lag	0.9597	0.9542	0.9500	0.0423	0.0450	0.0470	0.0171	0.0178	0.0192
		3-day-lag	0.9597	0.9493	0.9404	0.0422	0.0473	0.0513	0.0165	0.0186	0.0204
		4-day-lag	0.9586	0.9558	0.9533	0.0428	0.0442	0.0454	0.0186	0.0191	0.0196

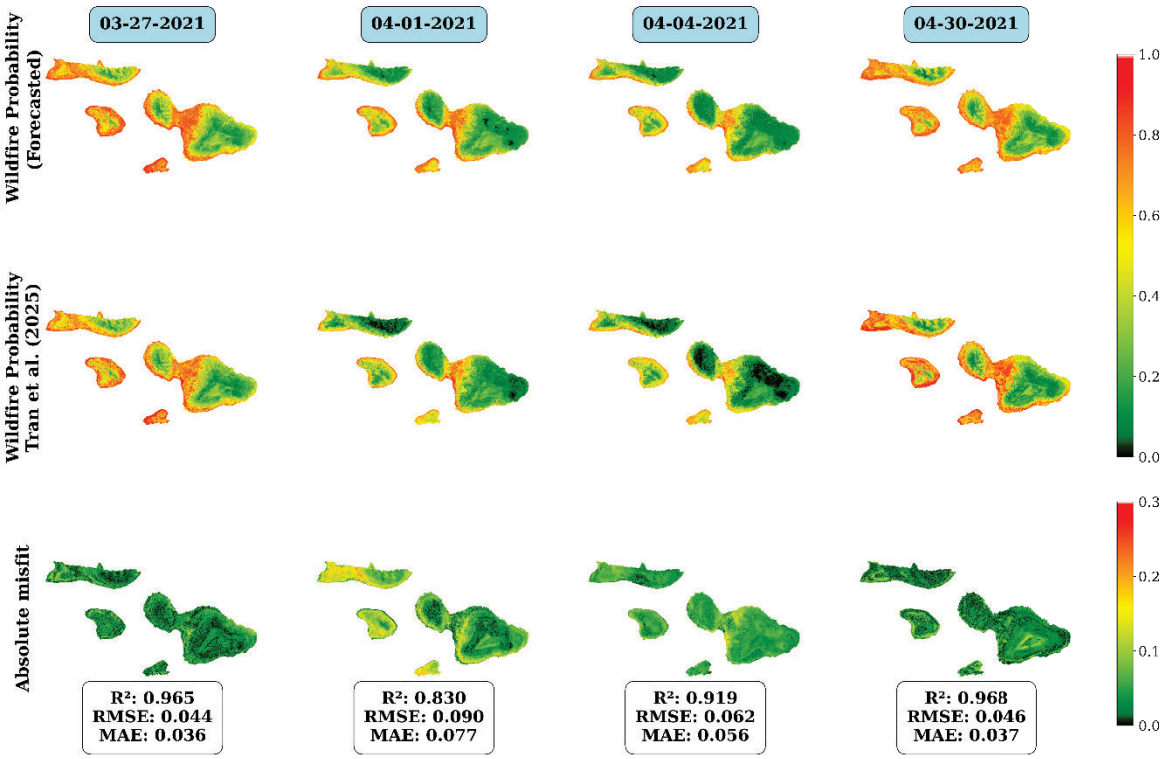

Figure 7. (Top row) 1-day ahead forecasted wildfire probability maps, (middle row) historical wildfire probability estimates from Tran et al. (2025), and (bottom row) the absolute misfit between the top and middle rows for four sample days in Maui County.

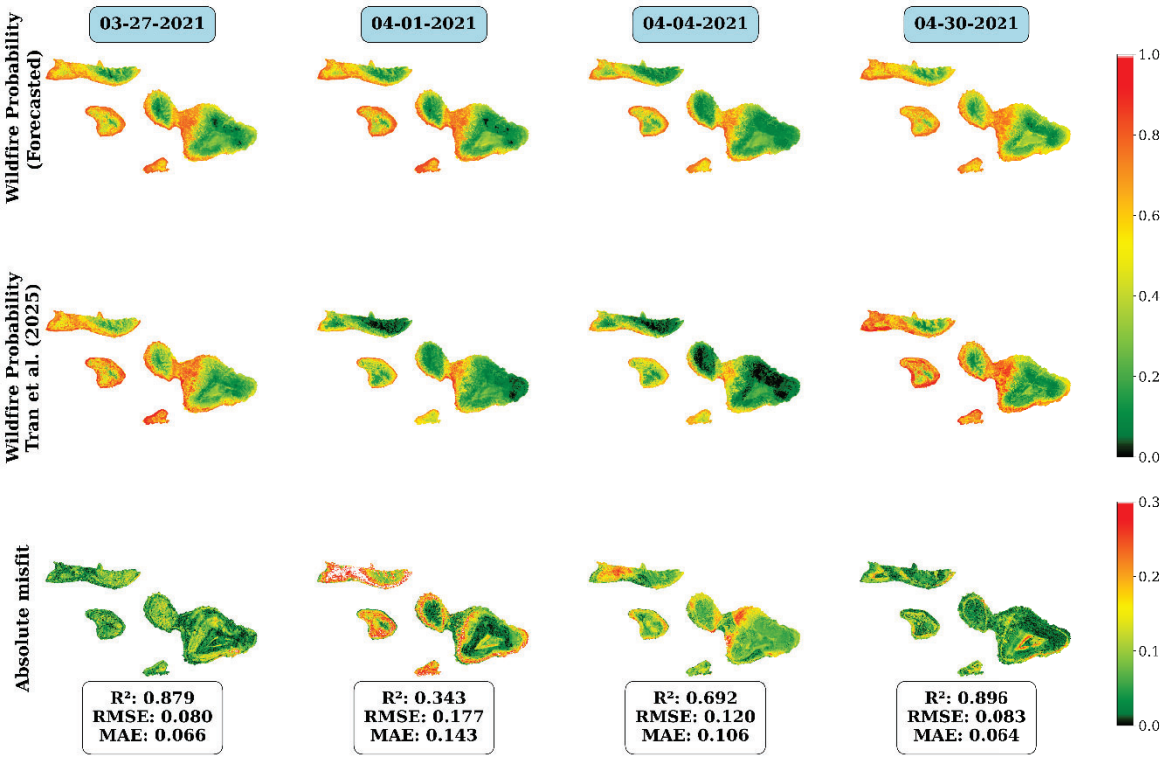

Figure 8. (Top row) 2-day ahead forecasted wildfire probability maps, (middle row) historical wildfire probability estimates from Tran et al. (2025), and (bottom row) the absolute misfit between the top and middle rows for four sample days in Maui County.

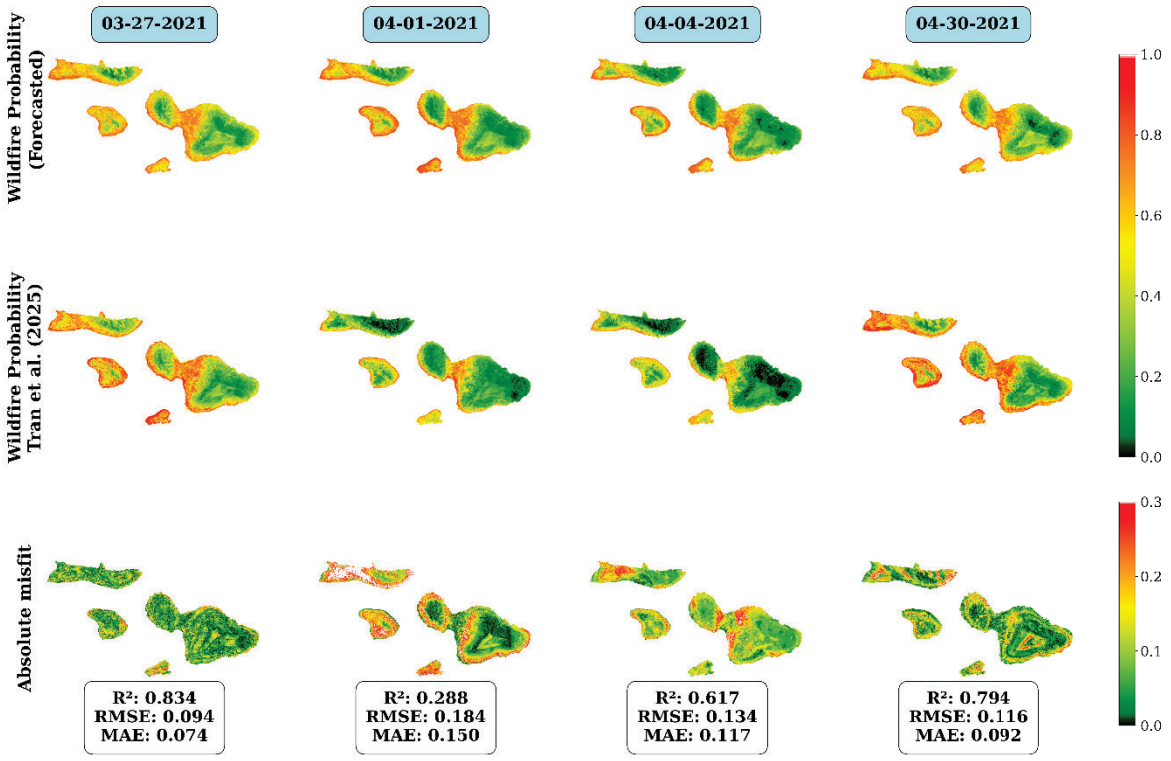

Figure 9. (Top row) 3-day ahead forecasted wildfire probability maps, (middle row) historical wildfire probability estimates from Tran et al. (2025), and (bottom row) the absolute misfit between the top and middle rows for four sample days in Maui County

Table 6 summarizes how the wildfire probability forecasts from the ConvLSTM and ConvLSTM-Attention models correspond to the wildfire events in Maui County during the testing phase. The ConvLSTM model shows sensitivity of 0.8000–0.8667, specificity of 0.6444–0.7111, NPV of 0.7805–0.8286, PPV of 0.6347–0.7264, F1-scores of 0.7551–0.7897, and AUC of 0.8108–0.8312 across the 1-, 2-, and 3-day forecasts for the three input configurations. The ConvLSTM-Attention model with a 4-day input lag provides the strongest overall agreement with the wildfire records, with the highest sensitivity values (0.8667–0.8778) and consistently high NPV and F1-scores (0.8209–0.8533 and 0.7757–0.8103), supported by AUC values of 0.8295–0.8731. These results indicate that adding attention improves wildfire detection capability for Maui, particularly at longer lead times where the ConvLSTM models show reduced performance. For the 4-day input lag, the ConvLSTM-Attention model increases sensitivity by 1.3–8.3%, specificity by 0–10.3%, NPV by 3.0–5.2%, PPV by 6.1–8.8%, F1-score by 0.9–3.9%, and AUC by 2.1–5.0% across the 1-, 2-, and 3-day forecasts compared to the ConvLSTM model.

Table 6. Comparison of forecasted wildfire probability maps for 1-, 2-, and 3-days ahead with the wildfire records for Maui County.

Metric indices	Lead time (day)	ConvLSTM			ConvLSTM-Attention		
		2-day-lag	3-day-lag	4-day-lag	2-day-lag	3-day-lag	4-day-lag
Sensitivity	1	0.8556	0.8222	0.8667	0.8333	0.8444	0.8778
	2	0.8556	0.8222	0.8222	0.8333	0.8778	0.8778
	3	0.8556	0.8222	0.8000	0.8333	0.9000	0.8667
Specificity	1	0.6778	0.6667	0.6444	0.7778	0.7444	0.7111
	2	0.6556	0.6444	0.7011	0.6667	0.6667	0.7067
	3	0.6889	0.6444	0.7111	0.6556	0.5556	0.7111
NPV	1	0.8243	0.7895	0.8286	0.8235	0.8272	0.8533
	2	0.8194	0.7838	0.8000	0.8000	0.8226	0.8308
	3	0.8267	0.7838	0.7805	0.8194	0.8475	0.8209
PPV	1	0.7264	0.7115	0.7091	0.7895	0.7677	0.7524
	2	0.7130	0.6781	0.6400	0.7143	0.6695	0.6870
	3	0.7033	0.6681	0.6347	0.7130	0.6694	0.6903
F1-score	1	0.7857	0.7629	0.7800	0.8108	0.8042	0.8103
	2	0.7678	0.7551	0.7689	0.7692	0.7596	0.7757
	3	0.7897	0.7551	0.7640	0.7678	0.7678	0.7785
AUC	1	0.8260	0.8221	0.8312	0.8538	0.8638	0.8731
	2	0.8108	0.8221	0.8135	0.8148	0.8128	0.8310
	3	0.8248	0.8247	0.8127	0.8167	0.8130	0.8295

Hawai‘i County

The forecasted wildfire probability maps for 1, 2, and 3 days ahead are compared with the historical wildfire probability maps from Tran et al. (2025) for Hawai‘i County in Table 7. The results show that both the ConvLSTM and ConvLSTM-Attention models achieved strong performance across all forecast horizons, with R^2 values above 0.88 for 1-day and 2-day forecasts and above 0.87 for the 3-day forecasts. The ConvLSTM-Attention model achieved R^2 values between 0.8840 and 0.9148 across the 2-, 3-, and 4-day lag

configurations, with RMSE ranging from 0.0631 to 0.0737 and MAE from 0.0297 to 0.0359. The 4-day-lag configuration performed best, reducing RMSE by 3.7%, 5.6%, and 5.2% for the 1-, 2-, and 3-day forecasts, respectively, when compared with the 2-day-lag model, and by 3.8%, 5.8%, and 5.4% for the same forecast horizons when compared with the 3-day-lag model. The corresponding MAE values were also lower, decreasing by 0.7%, 4.4%, and 3.1% for the 1-, 2-, and 3-day forecasts relative to the 2-day-lag model, and by 0.7%, 1.8%, and 0.6% when compared with the 3-day-lag model, indicating improved agreement with the historical wildfire probability maps. The ConvLSTM model showed a similar pattern, with the 4-day-lag configuration yielding the lowest RMSEs of 0.0633, 0.0682, and 0.0704 for respectively 1-, 2-, and 3-day ahead, further supporting the benefit of incorporating longer input sequences. Based on these improvements, the ConvLSTM-Attention model with a 4-day input lag was selected as the best-performing configuration.

The spatial comparisons for the selected dates (March 31, April 5, April 8, and April 15, 2021) are presented in Figures 10, 11, and 12, where the top row contains the forecasted wildfire probability, the middle row contains the wildfire probability map from the Tran et al. (2025) study, and the bottom row contains the absolute misfit between the forecasted and historical wildfire probability. These figures show that the ConvLSTM-Attention model with a 4-day lag represents the distribution of wildfire probability across Hawai‘i County well for the 1-, 2-, and 3-day forecasts. Tran et al. (2025) indicated higher wildfire probability in the northwestern, southern, and southeastern parts of the island on these dates, and these areas are well captured in the 1-, 2-, and 3-day forecasts. Figures 10, 11, and 12 indicate a clear increase in misfit as the forecast lead time extends from 1 to 3 days. April 8 presents the largest differences, particularly in the 3-day-ahead forecasts. Despite this increase, the misfit remains predominantly below 0.15, indicating relatively small differences compared with the wildfire-probability maps produced by Tran et al. (2025). The metrics support this agreement: R^2 values for the 1-day forecasts (Figure 10) range from 0.945 to 0.982, with RMSE between 0.031 and 0.046 and MAE between 0.024 and 0.036. For the 2-day forecasts (Figure 11), R^2 ranges from 0.761 to 0.886, RMSE from 0.078 to 0.097, and MAE from 0.056 to 0.073, while the 3-day forecasts (Figure 12) yield R^2 values between 0.728 and 0.875, RMSE from 0.081 to 0.103, and MAE from 0.060 to 0.078. These values show that the forecasts for Hawai‘i County match the wildfire-probability maps from the Tran et al. (2025) study across most dates, with reduced agreement only on April 8.

Table 7. Comparison of forecasted wildfire probability maps for 1-, 2-, and 3-day-ahead with the historical wildfire probability maps from Tran et al. (2025) for Hawai‘i County.

County	Model	Configuration	R^2			RMSE			MAE		
			1 day	2 days	3 days	1 day	2 days	3 days	1 day	2 days	3 days
Hawai‘i	ConvLSTM	2-day-lag	0.8957	0.8816	0.8748	0.0698	0.0744	0.0765	0.0338	0.0373	0.0390
		3-day-lag	0.9120	0.8997	0.8928	0.0641	0.0685	0.0708	0.0295	0.0329	0.0343
		4-day-lag	0.9143	0.9007	0.8942	0.0633	0.0682	0.0704	0.0351	0.0379	0.0394
	ConvLSTM-Attention	2-day-lag	0.9083	0.8906	0.8840	0.0655	0.0716	0.0737	0.0299	0.0344	0.0359
		3-day-lag	0.9139	0.8987	0.8913	0.0635	0.0689	0.0713	0.0299	0.0335	0.0350
		4-day-lag	0.9148	0.9023	0.8957	0.0631	0.0676	0.0699	0.0297	0.0329	0.0348

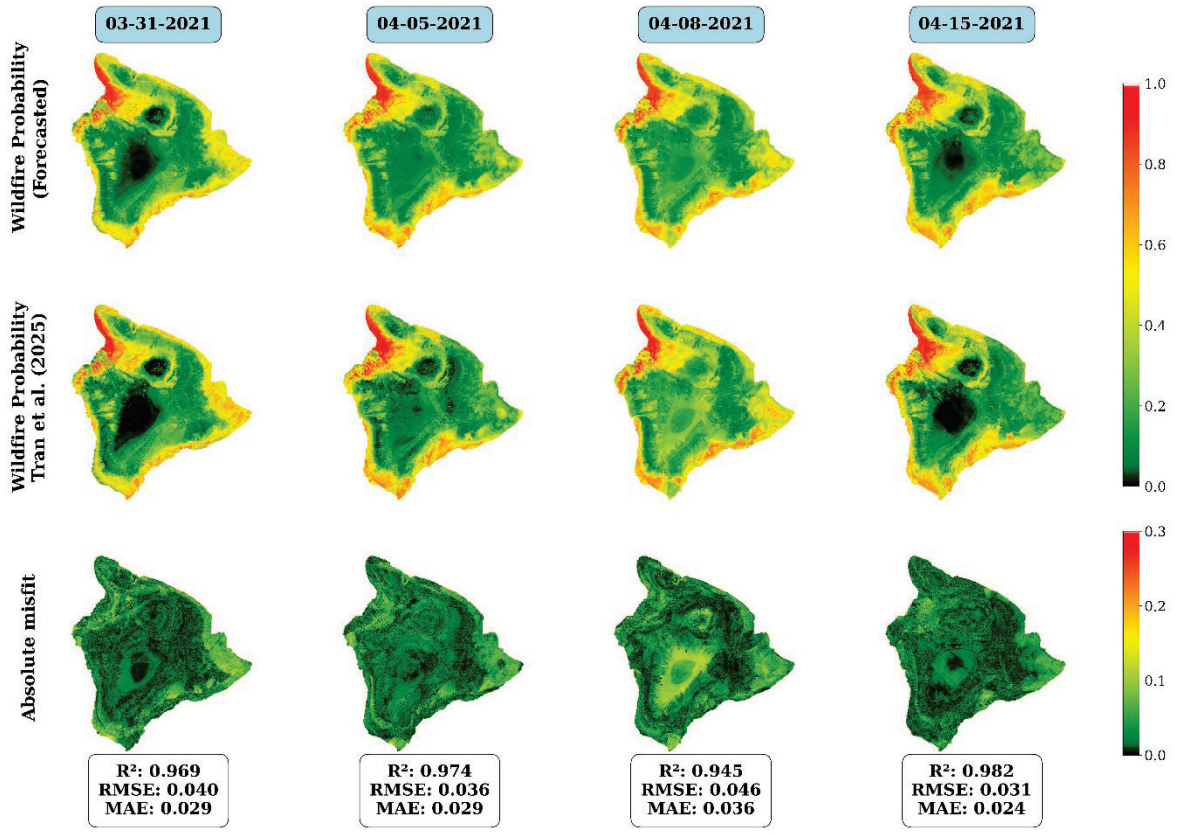

Figure 10. (Top row) 1-day ahead forecasted wildfire probability maps, (middle row) historical wildfire probability estimates from Tran et al. (2025), and (bottom row) the absolute misfit between the top and middle rows for four sample days in Hawai‘i County.

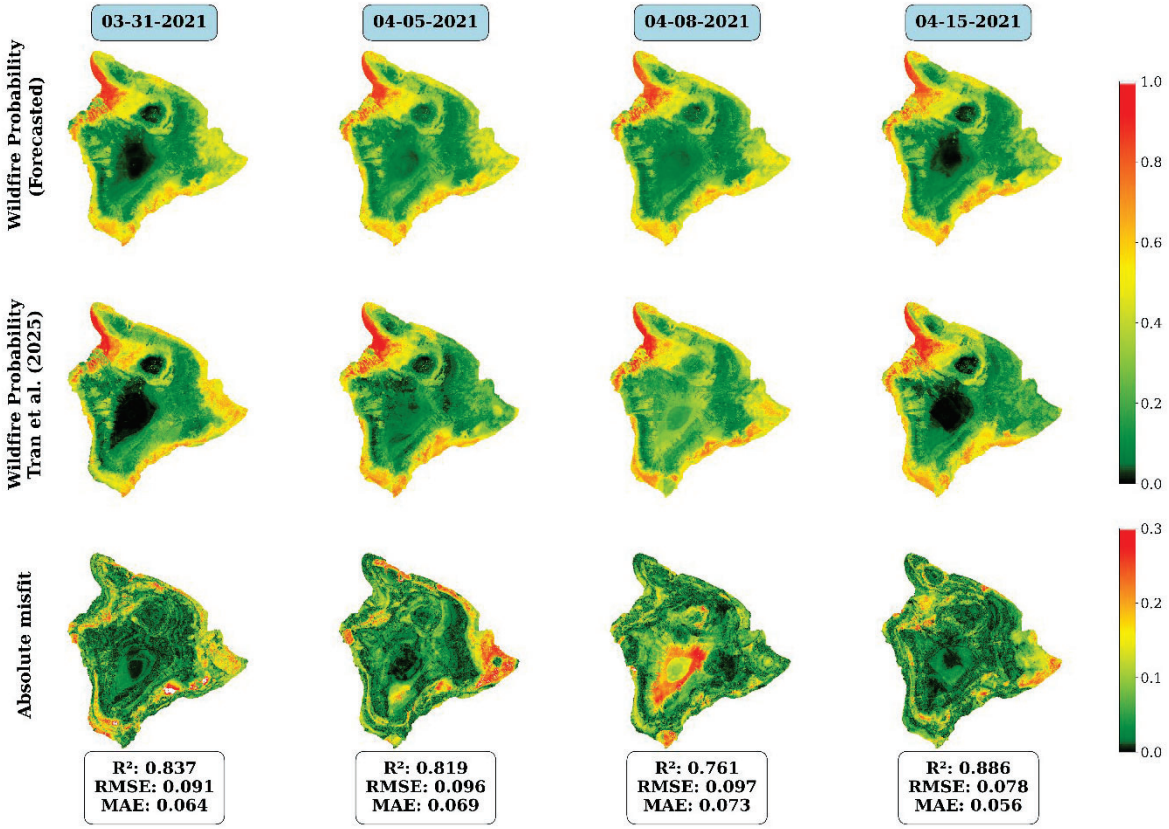

Figure 11. (Top row) 2-day ahead forecasted wildfire probability maps, (middle row) historical wildfire probability estimates from Tran et al. (2025), and (bottom row) the absolute misfit between the top and middle rows for four sample days in Hawai'i County.

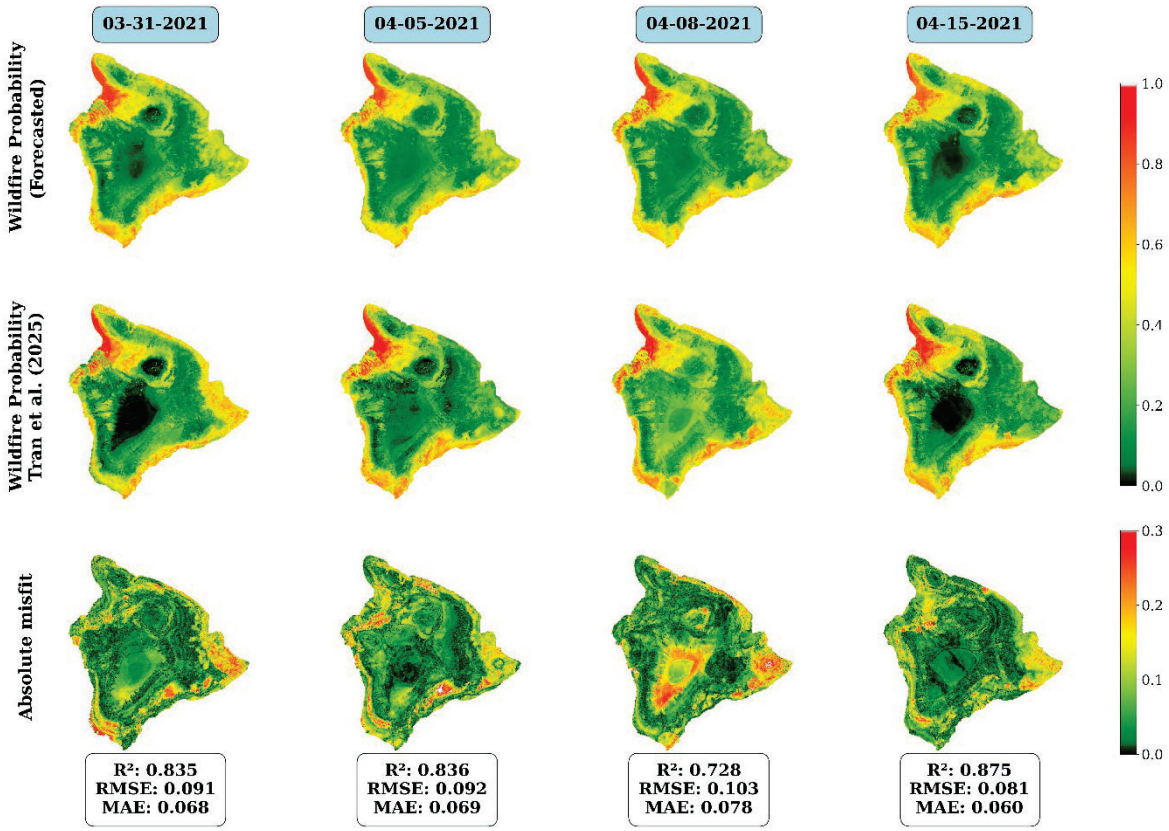

Figure 12. (Top row) 3-day ahead forecasted wildfire probability maps, (middle row) historical wildfire probability estimates from Tran et al. (2025), and (bottom row) the absolute misfit between the top and middle rows for four sample days in Hawai'i County.

Table 8 summarizes the correspondence between the forecasted wildfire probability maps and the observed wildfire occurrence during the testing phase for Hawai'i County across the 1-, 2-, and 3-day lead times. The ConvLSTM model shows sensitivity of 0.7181–0.7871, specificity of 0.7606–0.8191, NPV of 0.7424–0.7814, PPV of 0.7668–0.7988, F1-scores of 0.7486–0.7769, and AUC of 0.8265–0.8353 across the 1-, 2-, and 3-day forecast horizons. Among the tested configurations, the ConvLSTM-Attention model with a 4-day input lag provides the strongest agreement with the wildfire records, offering the highest sensitivity values across all lead times (0.7872–0.8138) and consistently high NPV and F1-score values (0.7802–0.8158 and 0.7849–0.8226), along with AUC of 0.8286–0.8636 across the 1-, 2-, and 3-day lead times. These results indicate that integrating attention mechanisms improves wildfire detection capability for Hawai'i County.

Across the forecast horizons, the 4-day-lag ConvLSTM-Attention model improves several key wildfire-identification metrics relative to the 4-day-lag ConvLSTM model. For the 1-day-ahead forecasts, sensitivity, specificity, NPV, PPV, F1-score, and AUC increased by 3.4%, 8.4%, 4.4%, 7.3%, 5.3%, and 3.8%, respectively. For the 2-day-ahead forecasts,

sensitivity, NPV, and F1-score increased by 5.7%, 3.5%, and 2.1%. For the 3-day-ahead forecasts, the same configuration increased sensitivity by 7.2%, NPV by 4.4%, and F1-score by 2.8%. These improvements highlight the contribution of the attention mechanism in strengthening wildfire detection across Hawai‘i County, especially at 1- and 3-day lead times where early identification is most critical for operational preparedness and response. These results show that although forecast accuracy decreases with longer lead times, the model maintains strong predictive capability and remains suitable for supporting wildfire early warning and risk management efforts on Hawai‘i Island.

Table 8. Comparison of forecasted wildfire probability maps for 1-, 2-, and 3-days ahead with the wildfire records for Hawai‘i County.

Model		ConvLSTM			ConvLSTM-Attention		
Metric indices	Lead time (day)	2-day-lag	3-day-lag	4-day-lag	2-day-lag	3-day-lag	4-day-lag
Sensitivity	1	0.7553	0.7766	0.7872	0.7979	0.7926	0.8138
	2	0.7287	0.7553	0.75	0.7606	0.7606	0.7926
	3	0.7181	0.7287	0.734	0.7553	0.7606	0.7872
Specificity	1	0.7979	0.7766	0.7606	0.8457	0.8351	0.8245
	2	0.8138	0.7766	0.7819	0.7819	0.766	0.7553
	3	0.8191	0.7819	0.7872	0.7766	0.766	0.7553
NPV	1	0.7653	0.7766	0.7814	0.8071	0.801	0.8158
	2	0.75	0.7604	0.7577	0.7656	0.7619	0.7845
	3	0.744	0.7424	0.7475	0.7577	0.7619	0.7802
PPV	1	0.7889	0.7766	0.7668	0.838	0.8278	0.8226
	2	0.7965	0.7717	0.7747	0.7772	0.7647	0.7641
	3	0.7988	0.7697	0.7753	0.7647	0.7647	0.7629
F1-score	1	0.7717	0.7766	0.7769	0.8174	0.8098	0.8182
	2	0.7611	0.7634	0.7622	0.7688	0.7627	0.7781
	3	0.7563	0.7486	0.7541	0.7596	0.7627	0.7749
AUC	1	0.8306	0.8353	0.8325	0.8599	0.8648	0.8639
	2	0.8286	0.8323	0.8269	0.8293	0.8292	0.8283
	3	0.8267	0.8328	0.8265	0.8291	0.8292	0.8286

Kauaʻi County

Table 9 summarizes the comparison between the 1-, 2-, and 3-day wildfire probability forecasts and the wildfire probability maps from Tran et al. (2025) for Kauaʻi County. Across different input-lag configurations, the ConvLSTM and ConvLSTM-Attention models reach R^2 values mostly above 0.84, with RMSE values between 0.0664 and 0.0832. For Kauaʻi County, the ConvLSTM-Attention model with a 4-day input lag produces the highest R^2 values—0.8944, 0.8894, and 0.8841 for the 1-, 2-, and 3-day forecasts. This configuration also yields the lowest RMSE (0.0664–0.0700). The 4-day-lag model shows RMSE reductions of 7.1%, 9.7%, and 8.0% for the 1-, 2-, and 3-day forecasts when compared with the 2-day-lag configuration, and reductions of 19.4%, 15.1%, and 15.9% when compared with the 3-day-lag configuration. For all three lead times, the 4-day-lag ConvLSTM-Attention model yields lower MAE values than the 4-day-lag ConvLSTM, with reductions of 4.27%, 7.27%, and 6.92% for the 1-, 2-, and 3-day forecasts, respectively. These comparisons show that the 4-day-lag ConvLSTM-Attention model provides the closest agreement with the wildfire probability estimates from Tran et al. (2025).

Figures 13, 14, and 15 present the spatial comparison for the selected dates (March 27, April 8, April 23, and June 25, 2021). In each figure, the top row contains the forecasted wildfire probability from the 4-day-lag ConvLSTM-Attention model for the corresponding lead time, the middle row contains the wildfire probability maps from Tran et al. (2025), and the bottom row contains the absolute misfit between the forecasted and historical wildfire probability. The Tran et al. (2025) maps indicate the highest wildfire probability in the western and northeastern parts of Kauaʻi, and our forecasts show strong agreement with these regions of higher wildfire probability. Figure 13, which presents the 1-day-ahead forecasts, shows low misfit across most of the island (R^2 = 0.950–0.971; RMSE = 0.032–0.046). Figure 14 presents the 2-day-ahead forecasts and shows larger differences—particularly on April 8 for which the misfit increases substantially (R^2 decreases to 0.260; RMSE increases to 0.122). Figure 15 indicates that the 3-day-ahead forecasts have higher misfit relative to shorter lead times. The forecasts span R^2 values from 0.243 with an RMSE of 0.123 on April 8 to 0.867 with an RMSE of 0.070 on June 25, reflecting the expected decrease in accuracy at longer horizons. Misfit values remain mostly below 0.2, and the high R^2 values for March 27, April 23, and June 25 (0.749, 0.880, and 0.867 respectively) for 3-day-ahead forecasts confirm strong agreement between the forecasts and the wildfire probability maps from Tran et al. (2025).

Table 9. Comparison of forecasted wildfire probability maps for 1-, 2-, and 3-day-ahead with the historical wildfire maps from Tran et al. (2025) for Kaua‘i County.

County	Model	Configuration	R^2			RMSE			MAE		
			1 day	2 days	3 days	1 day	2 days	3 days	1 day	2 days	3 days
Kaua‘i	ConvLSTM	2-day-lag	0.8803	0.8661	0.8635	0.0707	0.0750	0.0759	0.0431	0.0466	0.0471
		3-day-lag	0.8434	0.8391	0.8373	0.0809	0.0823	0.0830	0.0682	0.0680	0.0679
		4-day-lag	0.8656	0.8423	0.8360	0.0749	0.0815	0.0832	0.0468	0.0495	0.0506
	ConvLSTM-Attention	2-day-lag	0.8778	0.8646	0.8631	0.0715	0.0755	0.0761	0.0381	0.0405	0.0412
		3-day-lag	0.8375	0.8466	0.8364	0.0824	0.0803	0.0832	0.0500	0.0498	0.0523
		4-day-lag	0.8944	0.8894	0.8841	0.0664	0.0682	0.0700	0.0448	0.0459	0.0471

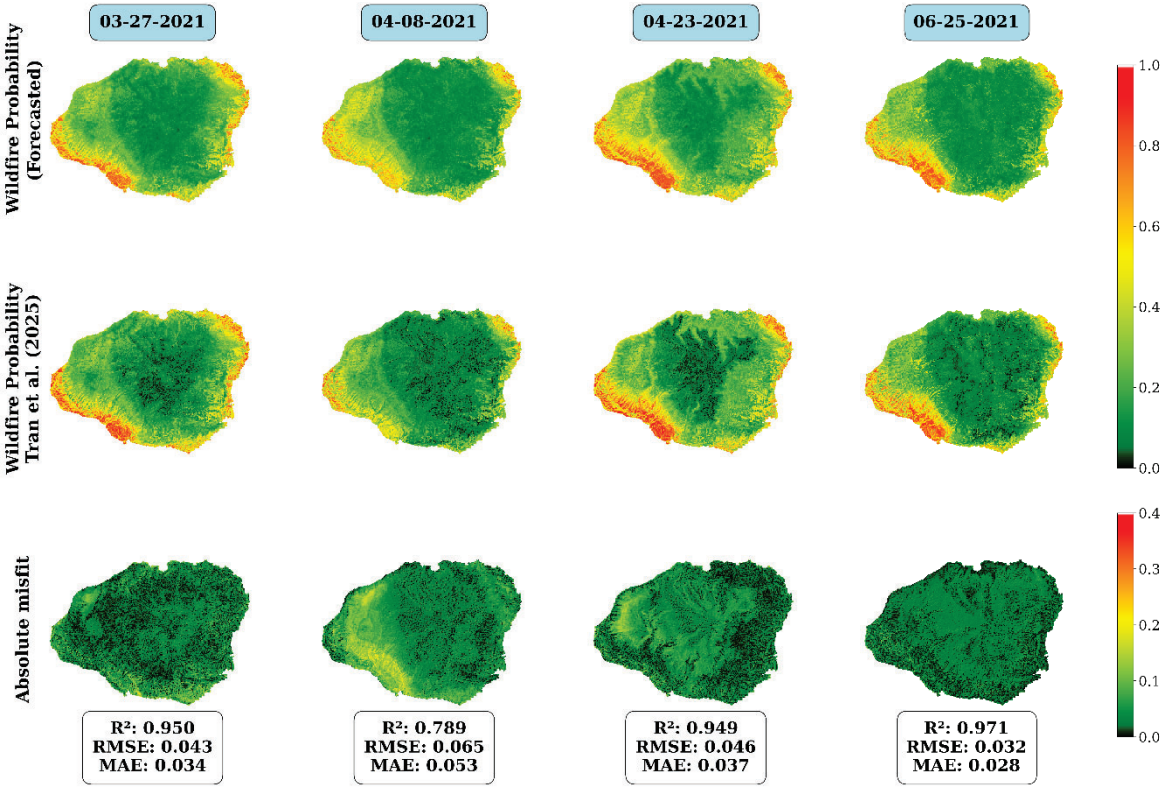

Figure 13. (Top row) 1-day ahead forecasted wildfire probability maps, (middle row) historical wildfire probability estimates from Tran et al. (2025), and (bottom row) the misfit between the top and middle rows for four sample days in Kaua‘i County.

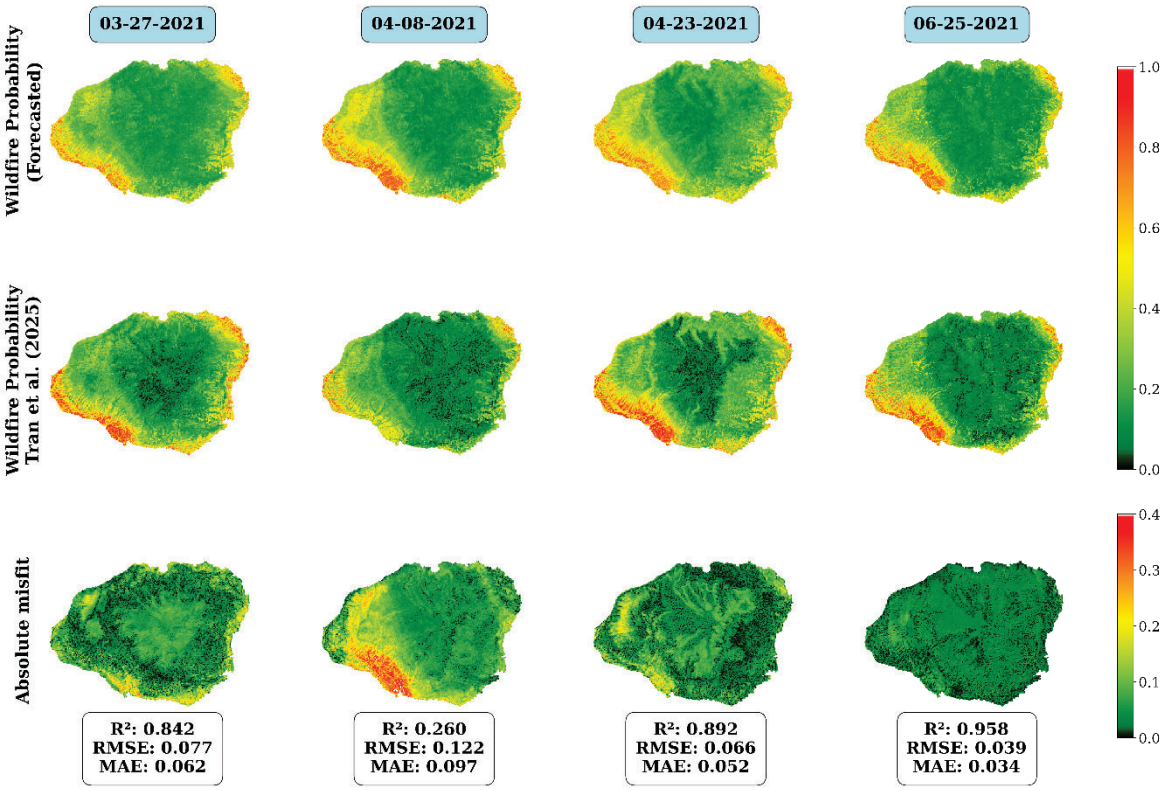

Figure 14. (Top row) 2-day ahead forecasted wildfire probability maps, (middle row) historical wildfire probability estimates from Tran et al. (2025), and (bottom row) the misfit between the top and middle rows for four sample days in Kaua'i County.

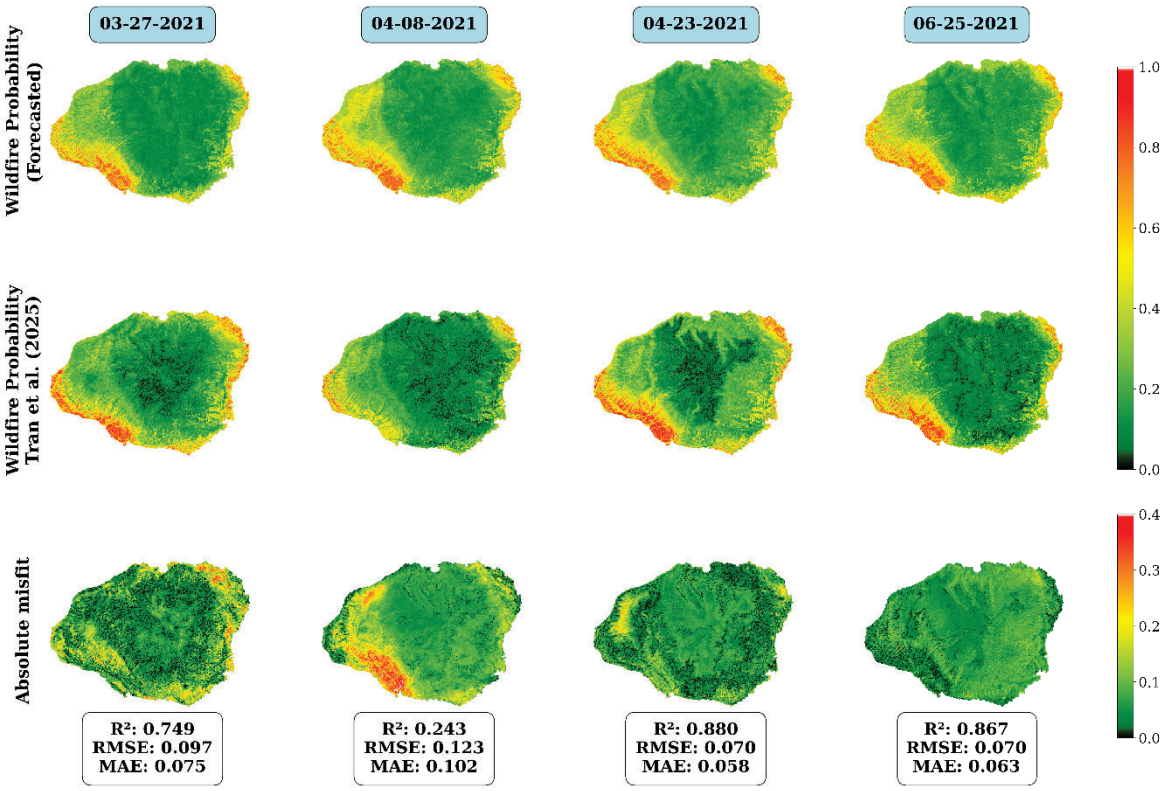

Figure 15. (Top row) 3-day ahead forecasted wildfire probability maps, (middle row) historical wildfire probability estimates from Trang et al. (2025), and (bottom row) the misfit between the top and middle rows for four sample days in Kaua'i County.

Table 10 summarizes the correspondence between the ConvLSTM and ConvLSTM-Attention forecasts and the observed wildfire occurrence during the testing phase for Kaua'i County across the 1-, 2-, and 3-day lead times. The ConvLSTM model shows sensitivity values of 0.6410–0.8077, specificity of 0.8205–0.8974, NPV of 0.7143–0.8101, PPV of 0.8108–0.8621, F1-scores of 0.7353–0.8129, and AUC of 0.8537–0.8729 across the 1–3 days forecasts. Among the two models, the ConvLSTM-Attention model with a 4-day input lag provides the strongest correspondence with the wildfire probability records, with the highest sensitivity values across all lead times (0.7821–0.8333) and consistently high F1-score and AUC values (0.7871–0.8387 and 0.8682–0.8964). The ConvLSTM-Attention model in all configurations show lower sensitivity and lower F1-scores at the 2-day and 3-day forecasts, indicating reduced ability to detect wildfire events at longer lead times. For the 1-day-ahead forecasts, the ConvLSTM-Attention model with a 4-day input lag increased sensitivity by 27.4%, NPV by 16.2%, F1-score by 13.5%, and AUC by 4.1% compared with the 4-day-lag ConvLSTM model. For the 2-day-ahead forecasts, the same configuration improved sensitivity by 28.0%, NPV by 14.2%, F1-score by 10.2%, and AUC by 0.9%. For the 3-day-ahead forecasts, sensitivity, NPV, F1-score, and AUC increased by 22.0%, 9.9%, 7.0%, and 1.2%, respectively. These improvements highlight the enhanced ability of the ConvLSTM-Attention model to identify wildfire events across all forecast horizons for Kaua'i County. These findings highlight the model's potential as a useful tool for early warning systems and proactive wildfire management, allowing for informed decision-making and resource allocation in fire-prone regions.

Table 10. Comparison of forecasted wildfire probability maps for 1-, 2-, and 3-days ahead with the wildfire records for Kaua‘i County.

Metric indices	Lead time (day)	ConvLSTM			ConvLSTM-Attention		
		2-day-lag	3-day-lag	4-day-lag	2-day-lag	3-day-lag	4-day-lag
Sensitivity	1	0.7692	0.8077	0.6538	0.8077	0.7436	0.8333
	2	0.7436	0.7692	0.641	0.8333	0.7821	0.8205
	3	0.7692	0.7436	0.641	0.8077	0.7692	0.7821
Specificity	1	0.8205	0.8205	0.8846	0.8205	0.8846	0.8462
	2	0.8333	0.8462	0.8974	0.7821	0.8077	0.7949
	3	0.8718	0.8718	0.8974	0.7821	0.7821	0.7949
NPV	1	0.7805	0.8101	0.7188	0.8101	0.7753	0.8354
	2	0.7647	0.7857	0.7143	0.8243	0.7875	0.8158
	3	0.7907	0.7727	0.7143	0.8026	0.7722	0.7848
PPV	1	0.8108	0.8182	0.85	0.8182	0.8657	0.8442
	2	0.8169	0.8333	0.8621	0.7927	0.8026	0.8000
	3	0.8571	0.8529	0.8621	0.7875	0.7792	0.7922
F1-score	1	0.7895	0.8129	0.7391	0.8129	0.8000	0.8387
	2	0.7785	0.8000	0.7353	0.8125	0.7922	0.8101
	3	0.8108	0.7945	0.7353	0.7975	0.7742	0.7871
AUC	1	0.8557	0.8711	0.8611	0.882	0.8695	0.8964
	2	0.8537	0.8729	0.8598	0.8600	0.8660	0.8679
	3	0.8549	0.8718	0.858	0.8585	0.8582	0.8682

Forecasting results for days with wildfire events

This section presents forecasting outcomes for the four Hawaiian counties on sample days that experienced wildfires and droughts. The goal was to evaluate the model’s ability to predict wildfires in advance and to assess how well its forecasts aligned with observed environmental dryness at the time of each fire event. To conduct this analysis, two days

with wildfire events were selected in each of the four Hawaiian counties, resulting in eight case studies. For each case, we assessed the model's ability to forecast wildfire probability at 1-, 2-, and 3-day lead times. Drought maps were also shown for these days.

For Honolulu County, we assessed the ConvLSTM-Attention model's performance for two wildfire events on July 3 and August 12, 2018. The fires on these dates had sizes of 0.1 and 1 acres, respectively. The wildfire locations for these two days are marked with stars in Figure 16. For both days, the model successfully forecasted high wildfire probability at the fire locations up to three days ahead. The forecasted fire maps consistently highlighted the southern, western, and southwestern parts of the island, known for receiving a small amount of rainfall, as high-risk zones. Drought maps for both days indicated moderate drought (D1) in the fire locations. The agreement between forecasted high-risk areas and dryness demonstrates the model's responsiveness to environmental stress (Figure 16).

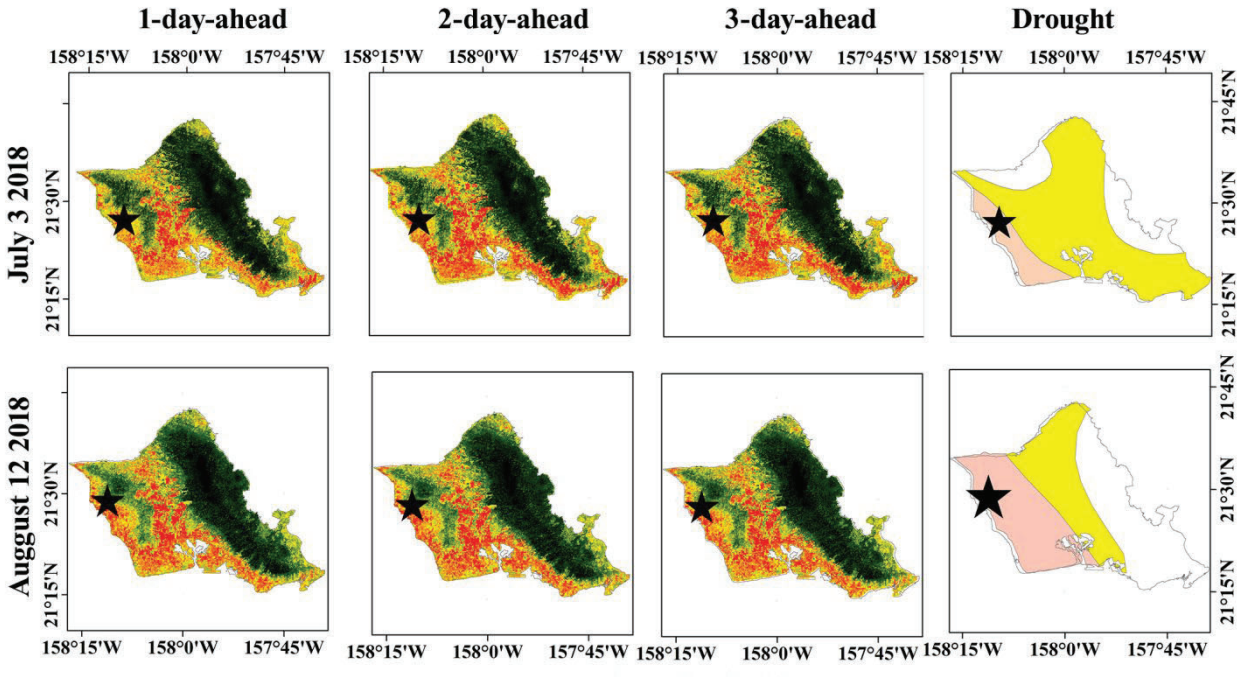

Figure 16. *Wildfire probability forecasts for Honolulu County on July 3 and August 12, 2018, at 1-, 2-, and 3-day lead times. Fire locations are marked with stars. Drought classifications are also shown for the same days.*

Figure 17 shows wildfire forecasts for Maui County on July 3 and August 12, 2018, along with the respective wildfire locations. One fire of 2,500 acres occurred on July 3, and two fires of 10 and 20 acres were observed on August 12. Across all lead times, the model consistently identified the fire locations as high-risk zones (shown in red), indicating high wildfire probability. This predictive consistency across three consecutive days underscores the robustness of the model, even at longer forecast horizons. The three fire events occurred under abnormal to moderate drought conditions (D0–D1), implying the environmental sensitivity of the model. Particularly, for August 12, the predicted high-risk

areas that experienced a wildfire fell within a region classified as moderate drought (D1), further validating the model's responsiveness to meteorological stressors.

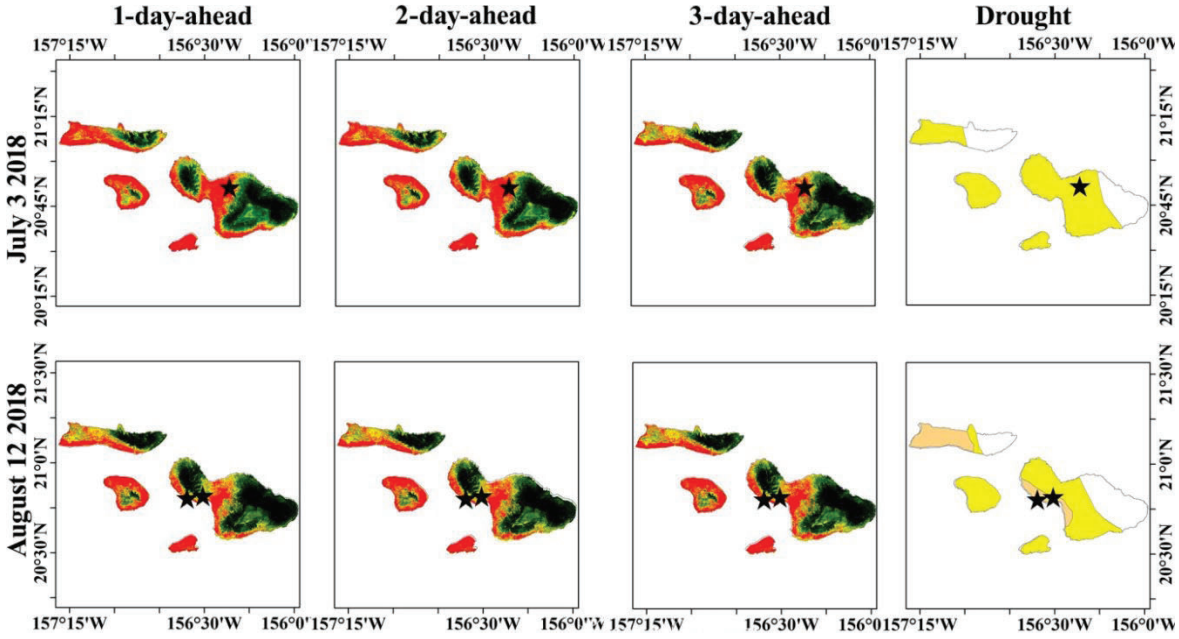

Figure 17. *Wildfire probability forecasts for Maui County on July 3 and August 12, 2018, at 1-, 2-, and 3-day lead times. Fire locations are marked with stars. Drought classifications are also shown for the same days.*

Wildfires forecasts for Hawai'i County are shown in Figure 18, for August 1, 2018 and October 3, 2019. Wildfires on these dates had the size of 18,000 and 130 acres, respectively. The model forecasted high wildfire probability at both fire locations across all lead times. The 2018 fire occurred in an area experiencing D0 to D1 drought, while the 2019 fire occurred within a zone of extreme drought (D3), surrounded by areas classified as D1 and D2. These results highlight the model's capability to detect high fire-risk under both moderate and severe drought conditions (Figure 18).

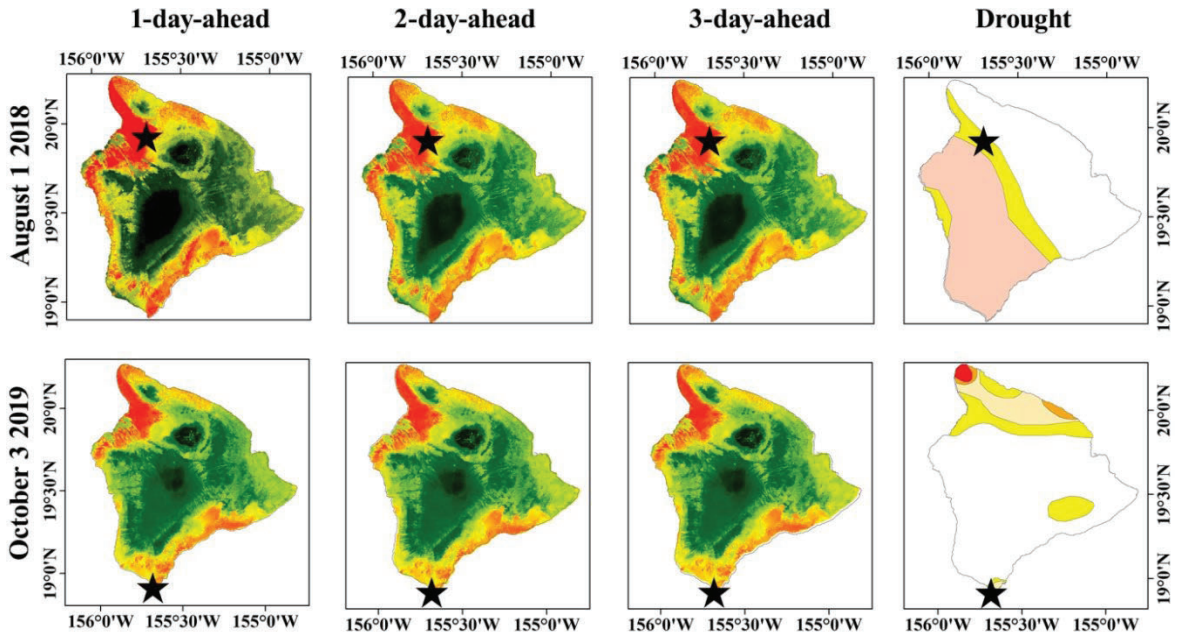

Figure 18. *Wildfire probability forecasts for Hawai'i County on August 1, 2018, and October 3, 2019, at 1-, 2-, and 3-day lead times. Fire locations are marked with stars. Drought classifications are also shown for the same days.*

For Kaua'i County, August 2, 2015, and June 19, 2019 were chosen as both days experienced wildfires. Three fires of 0.01, 0.01, and 25 acres were recorded on August 2, and two fires of 0.01 and 2000 acres happened on June 19. The largest fires on these dates (i.e., the 25-acre fire on August 2, 2015 and the 2000-acre fire on June 19, 2019) are marked with stars in Figure 19. For August 2, the model forecasted high probability at the fire locations, which were situated within a D2 (severe drought) zone. For June 19, the fire occurred near the boundary between moderate (D1) and severe drought (D2), which was captured by the model's high-risk fire forecasts across all lead times (Figure 19).

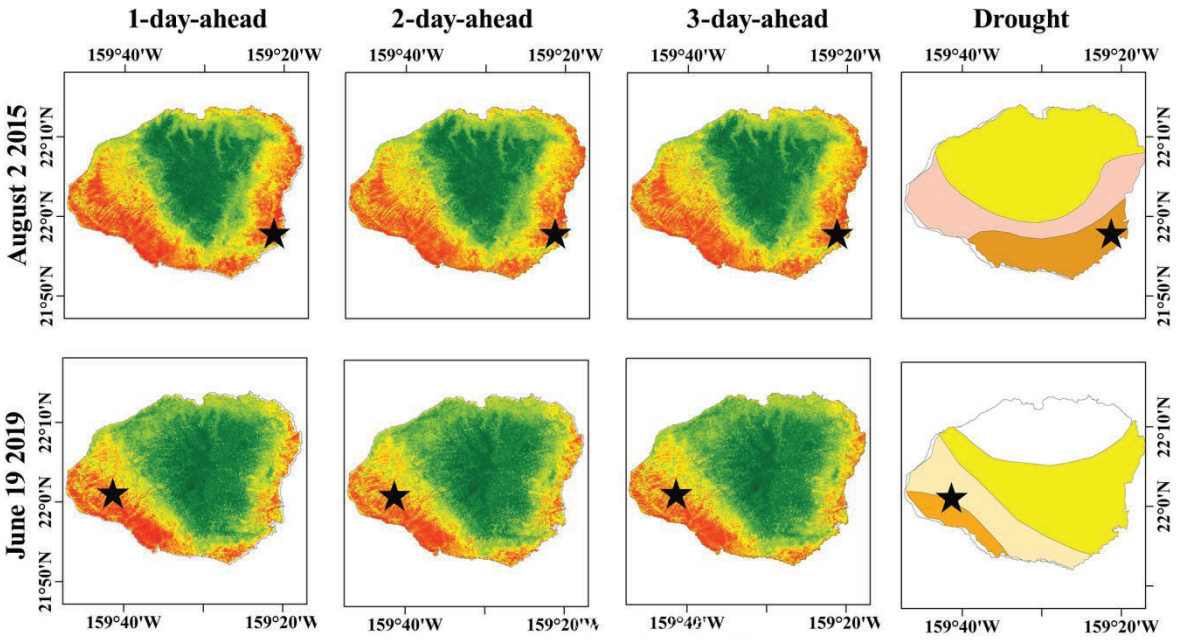

Figure 19. *Wildfire probability forecasts for Kaua'i County on August 2, 2015, and June 19, 2019, at 1-, 2-, and 3-day lead times. Fire locations are marked with stars. Drought classifications are also shown for the same days.*

Overall, results across all four Hawaiian counties and all selected dates show that the model generates satisfactory wildfire forecasts. Its ability to flag high-risk zones a few days ahead demonstrates clear potential for deployment in real-time wildfire early warning systems. This predictive capability represents a significant advancement in data-driven fire risk management for drought-sensitive regions such as the Hawaiian Islands.

In August 2023, the Hawai'i Wildfires (also known as the Maui Wildfires) caused more than 100 deaths and damaged or destroyed around 3,000 buildings, leading to the deadliest wildfire in the U.S. in more than a century (NOAA/NCEI, 2024). The fires inflicted the most significant damage on the historic town of Lāhainā, and to a lesser extent in Upper Kula, as shown in Figure 20 by black polygons. To further evaluate the model performance, we plotted wildfire risk forecast maps for 1-, 2-, and 3-day ahead during the extreme wildfire event for Maui County in August 2023. The locations of these wildfires are shown in Figure 20. Remarkably, wildfire forecast maps from August 8 to August 11 consistently indicated very high wildfire probabilities in Lahaina and Kula. Moreover, the U.S. Drought Monitor maps for August 8 and August 15 show that Lāhainā and Upper Kula was experiencing moderate (D1) to severe (D2) drought, highlighting the consistency of forecasted wildfire risk with short-term drought dynamics and reinforces its operational value in early warning applications. According to the U.S. Drought Monitor framework, such drought classifications are associated with meteorological and agricultural drought types. These conditions involve precipitation deficits, elevated evaporative demand, and soil moisture depletion, all of which critically enhance fuel flammability and fire potential. These results are consistent with recent studies

emphasizing the effect of drought on wildfires, including the work of Richardson et al. (2022) and Yin et al. (2024).

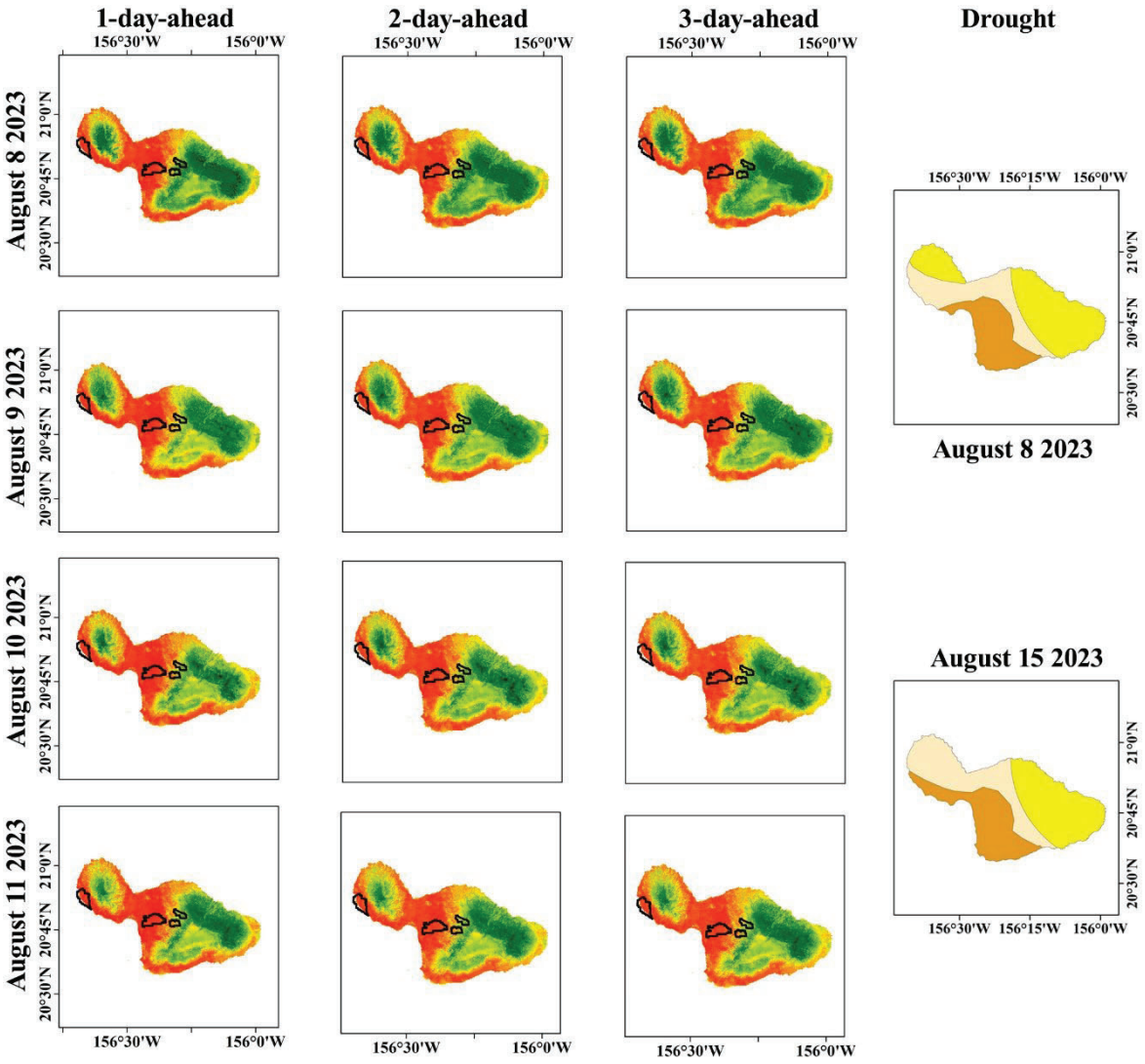

Figure 20. *Wildfire probability forecasts for 1, 2, and 3-day ahead for Maui Island from August 8 to 11, 2023 as well as corresponding drought classification maps*

Discussion

The results of this study underscore the potential of deep learning models, particularly the ConvLSTM framework enhanced with attention mechanisms, for improving wildfire forecasting in the Hawaiian Islands. These findings are consistent with prior research that highlights the value of advanced machine learning approaches in fire risk assessment. For instance, Tran et al. (2025) showed that integrating the RF model with metaheuristic optimization techniques can improve near real-time wildfire probability estimation. The present study advances Tran et al. (2025)'s near real-time wildfire risk prediction to near-future prediction. The ConvLSTM-Attention model offers superior forecasting accuracy by

more effectively capturing both spatial and temporal patterns. The results suggest that deep learning architectures, especially those designed for sequential data, may outperform traditional machine learning methods in forecasting wildfire dynamics.

Recent studies, including those by Yelenik et al. (2024) and Mass and Ovens (2024), have documented the rising frequency of wildfires in Hawai‘i, attributing this trend to climate change, the spread of invasive vegetation, and human activities. The present study contributes to the existing literature by presenting a predictive framework, which enables short-term wildfire forecasting. The integration of attention mechanisms in the ConvLSTM model plays a crucial role in improving predictive accuracy. Similar findings have been reported in other domains, such as precipitation forecasting (Shi et al., 2015) and natural disaster forecast (Rahman and Siddiqui, 2019), where attention-enhanced LSTMs have shown improved performance in handling spatiotemporal dependencies. at For the 1-day-ahead forecasts, the F1-score from the 4-day-lag ConvLSTM-Attention model increases by 2.66% for Honolulu County, 5.32% for Hawai‘i County, 3.88% for Maui County, and 13.48% for Kaua‘i County, relative to the 4-day-lag ConvLSTM. This aligns with previous work by Vaswani et al. (2017), who demonstrated that attention mechanisms enhance neural networks' ability to prioritize critical information in sequence-based learning tasks.

In this study, we utilized sequences of wildfire probabilities produced by Tran et al. (2025) as inputs into the ConvLSTM-Attention model. These wildfire sequences were already obtained by utilizing key environmental factors including maximum air temperature, relative humidity, rainfall, NDVI, antecedent precipitation index (API), and land cover into a RF model. Future research could expand the current framework by incorporating additional influential variables such as soil moisture (Yelenik et al., 2024) and fuel load characteristics (Jacobi et al., 2017) in the ConvLSTM-Attention model to further improve forecast precision. Therefore, while core weather and vegetation indices (i.e., maximum air temperature, relative humidity, rainfall, NDVI, antecedent precipitation index (API), and land cover) were considered, incorporating more influential input data enhance the model's accuracy. Moreover, ensemble approaches combining multiple deep learning architectures, as suggested by Tehrany et al. (2019), may further strengthen performance by leveraging diverse modeling strategies. Our use of a hybrid ConvLSTM model with attention mechanisms has effectively captured spatiotemporal dependencies, yet future research may explore further enhancements to improve generalization and robustness across varying time scales and regions.

The ability to generate high-resolution predictive wildfire maps provides valuable tools for emergency responders, land-use planners, and policymakers. By enabling proactive decision-making, the proposed model supports targeted fire prevention strategies, early evacuation planning, and optimized resource allocation key factors in reducing wildfire impacts (Thompson et al., 2019). In conclusion, our study demonstrates that a ConvLSTM-Attention model enhances wildfire forecasting accuracy, outperforming traditional models in short-term forecasts.

Conclusion

This study develops a hybrid deep learning framework that integrates ConvLSTM with attention mechanisms, optimized by the Firefly Algorithm, to forecast wildfire probabilities across the four Hawaiian counties. By leveraging multi-day input sequences, the proposed model achieves high spatial and temporal accuracy, providing wildfire forecasts up to three days in advance.

Our wildfire forecasts demonstrate strong agreement with the wildfire-probability maps of Tran et al. (2025), with R^2 values exceeding 0.88 across all forecast lead times and all four counties—Honolulu, Maui, Hawai‘i, and Kaua‘i. RMSE values were consistently below 0.07 and MAE values below 0.047 across all counties and lead times. This shows that the model forecasts wildfire satisfactorily and in strong agreement with the wildfire patterns presented by Tran et al. (2025).

Validation against recorded wildfire events indicates the reliability of the model in identifying fire-prone areas. Additionally, drought condition maps from the U.S. Drought Monitor were used to assess forecasted fire-prone zones, revealing strong spatial alignment between predicted fire risk and areas experiencing drought. This correspondence highlights the influence of environmental dryness on wildfire activity and provides ecological support for the model’s outputs. The addition of an attention mechanism to ConvLSTM improved the 1-day-ahead forecasts, increasing the F1-score by 2.7% in Honolulu County, 5.3% in Hawai‘i County, 3.9% in Maui County, and 13.5% in Kaua‘i County, with corresponding AUC increases of 3.1%, 3.8%, 5.9%, and 4.1%, respectively. These improvements reflect the model's enhanced ability to extract meaningful spatiotemporal features and distinguish high-risk fire zones under varying environmental conditions.

Differences in performance across counties suggest that incorporating additional environmental variables such as soil moisture and fuel load could further enhance forecasting accuracy. Overall, this project demonstrates the effectiveness of attention-based deep learning for short-term wildfire forecasting. High-resolution wildfire-probability forecasts enable early detection of fire conditions and provide practical information for land-management planning, emergency response, and policy development.

References

Ares, A., Fownes, J.H., 2000. Productivity, nutrient and water-use efficiency of Eucalyptus saligna and Toona ciliata in Hawaii. For. Ecol. Manage. 139. https://doi.org/10.1016/S0378-1127(00)00270-X

Bahdanau, D., Cho, K.H., Bengio, Y., 2015. Neural machine translation by jointly learning to align and translate, in: 3rd International Conference on Learning Representations, ICLR 2015 - Conference Track Proceedings.

Blumenstock, D.I., Price, S., 1994. Climates of the States: Hawaii, in: A Natural History of the Hawaiian Islands. University of Hawaii Press, pp. 94–114. https://doi.org/10.1515/9780824844264-008

Burgan, R.E., Fujioka, F.M., Hirata, G.H., 1974. A fire danger rating system for Hawaii. Fire Technol. 10. https://doi.org/10.1007/BF02589985

Chu, P.S., 1995. Hawaii rainfall anomalies and El Nino. J. Clim. 8. https://doi.org/10.1175/1520-0442(1995)008<1697:HRAAEN>2.0.CO;2

Chu, P.S., Yan, W., Fujioka, F., 2002. Fire-climate relationships and long-lead seasonal wildfire prediction for Hawaii. Int. J. Wildl. Fire 11. https://doi.org/10.1071/WF01040

Dolling, K., Chu, P.-S., Fujioka, F., 2009. Natural variability of the Keetch–Byram drought index in the Hawaiian Islands. Int. J. Wildl. fire 18, 459–475.

Fister, I., Yang, X.S., Brest, J., 2013. A comprehensive review of firefly algorithms. Swarm Evol. Comput. 13. https://doi.org/10.1016/j.swevo.2013.06.001

Frazier, A.G., Giambelluca, T.W., 2017. Spatial trend analysis of Hawaiian rainfall from 1920 to 2012. Int. J. Climatol. 37. https://doi.org/10.1002/joc.4862

Fujioka, F.M., Weise, D.R., Burgan, R.E., 2000. A high resolution fire danger rating system for Hawaii, in: 3rd Symposium on Fire and Forest Meteorology. pp. 9–14.

Giambelluca, T.W., Chen, Q., Frazier, A.G., Price, J.P., Chen, Y.-L., Chu, P.-S., Eischeid, J.K., Delparte, D.M., 2013. Online rainfall atlas of Hawai ‘i. Bull. Am. Meteorol. Soc. 94, 313–316.

Giambelluca, T.W., Diaz, H.F., Luke, M.S.A., 2008. Secular temperature changes in Hawai’i. Geophys. Res. Lett. 35. https://doi.org/10.1029/2008GL034377

Hai, T., Theruvil Sayed, B., Majdi, A., Zhou, J., Sagban, R., Band, S.S., Mosavi, A., 2023. An integrated GIS-based multivariate adaptive regression splines-cat swarm optimization for improving the accuracy of wildfire susceptibility mapping. Geocarto Int. https://doi.org/10.1080/10106049.2023.2167005

Hamadeh, N., Karouni, A., Daya, B., Chauvet, P., 2017. Using correlative data analysis to develop weather index that estimates the risk of forest fires in Lebanon & Mediterranean: Assessment versus prevalent meteorological indices. Case Stud. Fire Saf. 7. https://doi.org/10.1016/j.csfs.2016.12.001

Hand, D.J., 2009. Measuring classifier performance: A coherent alternative to the area under the ROC curve. Mach. Learn. 77. https://doi.org/10.1007/s10994-009-5119-5

Hantson, S., Pueyo, S., Chuvieco, E., 2015. Global fire size distribution is driven by human impact and climate. Glob. Ecol. Biogeogr. 24. https://doi.org/10.1111/geb.12246

Jacobi, J.D., Price, J.P., Fortini, L.B., Gon III, S.M., Berkowitz, P., 2017. Hawaii land cover and habitat status: US Geological Survey data release. US Geol. Surv. Moffett Field, California, USA.

Kalantar, B., Ueda, N., Idrees, M.O., Janizadeh, S., Ahmadi, K., Shabani, F., 2020. Forest fire susceptibility prediction based on machine learning models with resampling algorithms on remote sensing data. Remote Sens. 12. https://doi.org/10.3390/rs12223682

Larabi Marie-Sainte, S., Alalyani, N., 2020. Firefly Algorithm based Feature Selection for Arabic Text Classification. J. King Saud Univ. - Comput. Inf. Sci. 32. https://doi.org/10.1016/j.jksuci.2018.06.004

Li, Y., Li, J., Sun, Y., Li, H., 2022. Load Balancing Based on Firefly and Ant Colony Optimization Algorithms for Parallel Computing. Biomimetics 7. https://doi.org/10.3390/biomimetics7040168

Longman, R.J., Frazier, A.G., Newman, A.J., Giambelluca, T.W., Schanzenbach, D., Kagawa-Viviani, A., Needham, H., Arnold, J.R., Clark, M.P., 2019. High-resolution gridded daily rainfall and temperature for the Hawaiian Islands (1990-2014). J. Hydrometeorol. 20. https://doi.org/10.1175/JHM-D-18-0112.1

Lucas, M., 2017. Spatially Quantifying and Attributing 17 Years of Vegetation and Land Cover Transitions Across Hawaii. University of Hawai`i at Manoa, Honolulu.

Madson, A., Dimson, M., Fortini, L.B., Kawelo, K., Ticktin, T., Keir, M., Dong, C., Ma, Z., Beilman, D.W., Kay, K., Ocón, J.P., Gallerani, E., Pau, S., Gillespie, T.W., 2023. A Near Four-Decade Time Series Shows the Hawaiian Islands Have Been Browning Since the 1980s. Environ. Manage. 71. https://doi.org/10.1007/s00267-022-01749-x

Marris, E., 2023. Hawaii wildfires: did scientists expect Maui to burn? Nature. https://doi.org/10.1038/d41586-023-02571-z

Mass, C., Ovens, D., 2024. The meteorology of the August 2023 Maui wildfire. Weather Forecast. 39, 1097–1115.

McCaffrey, S., 2015. Community wildfire preparedness: A global state-of-the-knowledge summary of social science research. Curr. For. Reports 1. https://doi.org/10.1007/s40725-015-0015-7

Mnih, V., Heess, N., Graves, A., Kavukcuoglu, K., 2014. Recurrent models of visual attention, in: Advances in Neural Information Processing Systems.

Moishin, M., Deo, R.C., Prasad, R., Raj, N., Abdulla, S., 2021. Designing deep-based learning flood forecast model with ConvLSTM hybrid algorithm. IEEE Access 9. https://doi.org/10.1109/ACCESS.2021.3065939

Naidu, G., Zuva, T., Sibanda, E.M., 2023. A Review of Evaluation Metrics in Machine Learning Algorithms, in: Lecture Notes in Networks and Systems. https://doi.org/10.1007/978-3-031-35314-7_2

Nayak, J., Naik, B., Dinesh, P., Vakula, K., Dash, P.B., 2020. Firefly Algorithm in

Biomedical and Health Care: Advances, Issues and Challenges. SN Comput. Sci. https://doi.org/10.1007/s42979-020-00320-x

NOAA/NCEI, 2024. U.S. Billion-Dollar Weather and Climate Disasters [WWW Document]. NOAA Natl. Centers Environ. Inf.

Noel, M., Bathke, D., Fuchs, B., Gutzmer, D., Haigh, T., Hayes, M., Poděbradská, M., Shield, C., Smith, K., Svoboda, M., 2020. Linking drought impacts to drought severity at the state level. Bull. Am. Meteorol. Soc. 101. https://doi.org/10.1175/BAMS-D-19-0067.1

Pandey, S., Kumari, N., Dash, S.K., Nawajish, S. Al, 2022. Challenges and monitoring methods of forest management through geospatial application: A review, in: Advances in Remote Sensing for Forest Monitoring. https://doi.org/10.1002/9781119788157.ch13

Perroy, R.L., Melrose, J., Cares, S., 2016. The evolving agricultural landscape of post-plantation Hawai'i. Appl. Geogr. 76. https://doi.org/10.1016/j.apgeog.2016.09.018

Pilly Joseph Kagosi, Siwa Ernest Nkya, Chelestino Peter Balama, Innocent Hamisi Babili, 2020. Effectiveness of Firewise Approach (FWA) in Controlling Forest Fire: A Case of Uluguru Nature Forest Reserve (UNFR), Morogoro, Tanzania. J. Agric. Sci. Technol. B 10. https://doi.org/10.17265/2161-6264/2020.03.006

Rahman, M.M., Siddiqui, F.H., 2019. An optimized abstractive text summarization model using peephole convolutional LSTM. Symmetry (Basel). 11. https://doi.org/10.3390/sym11101290

Rezaie, F., Panahi, M., Bateni, S.M., Lee, S., Jun, C., Trauernicht, C., Neale, C.M.U., 2023. Development of novel optimized deep learning algorithms for wildfire modeling: A case study of Maui, Hawai'i. Eng. Appl. Artif. Intell. 125. https://doi.org/10.1016/j.engappai.2023.106699

Richardson, D., Black, A.S., Irving, D., Matear, R.J., Monselesan, D.P., Risbey, J.S., Squire, D.T., Tozer, C.R., 2022. Global increase in wildfire potential from compound fire weather and drought. npj Clim. Atmos. Sci. 5. https://doi.org/10.1038/s41612-022-00248-4

Shi, X., Chen, Z., Wang, H., Yeung, D.Y., Wong, W.K., Woo, W.C., 2015. Convolutional LSTM network: A machine learning approach for precipitation nowcasting, in: Advances in Neural Information Processing Systems.

Tehrany, M.S., Jones, S., Shabani, F., Martínez-Álvarez, F., Tien Bui, D., 2019. A novel ensemble modeling approach for the spatial prediction of tropical forest fire susceptibility using LogitBoost machine learning classifier and multi-source geospatial data. Theor. Appl. Climatol. 137. https://doi.org/10.1007/s00704-018-2628-9

Thompson, M.P., Wei, Y., Calkin, D.E., O'Connor, C.D., Dunn, C.J., Anderson, N.M., Hogland, J.S., 2019. Risk Management and Analytics in Wildfire Response. Curr. For. Reports. https://doi.org/10.1007/s40725-019-00101-7

Tran, T.T.K., Bateni, S., Lucas, M., Kodama, K., Janizadeh, S., Vosoughifar, H., Trauernicht, C., Longman, R., Giambelluca, T.W., Kourkchi, E., McLean, J., Cleveland, S., Morioka, B., 2025. Developing a Near Real-Time Wildfire System for the State of Hawai'i, Submitted to Expert Systems.

Trauernicht, C., 2019. Vegetation—Rainfall interactions reveal how climate variability and climate change alter spatial patterns of wildland fire probability on Big Island, Hawaii. Sci. Total Environ. 650. https://doi.org/10.1016/j.scitotenv.2018.08.347

Trauernicht, C., 2015. El Niño and Long-Lead Fire Weather Prediction for Hawaii and Us-Affiliated Pacific Islands. Pacific Fire Exch. (PFX), PFX Fact Sheet 2015_1.

Trauernicht, C., Pickett, E., Giardina, C.P., Litton, C.M., Cordell, S., Beavers, A., 2015. The contemporary scale and context of wildfire in Hawai 'i1. Pacific Sci. 69, 427–444.

Umberger, R.A., Hatfield, L.A., Speck, P.M., 2017. Understanding Negative Predictive Value of Diagnostic Tests Used in Clinical Practice. Dimens. Crit. Care Nurs. 36. https://doi.org/10.1097/DCC.0000000000000219

Vaswani, A., Shazeer, N., Parmar, N., Uszkoreit, J., Jones, L., Gomez, A.N., Kaiser, Ł., Polosukhin, I., 2017. Attention is all you need, in: Advances in Neural Information Processing Systems.

Wardhani, N.W.S., Rochayani, M.Y., Iriany, A., Sulistyono, A.D., Lestantyo, P., 2019. Cross-validation Metrics for Evaluating Classification Performance on Imbalanced Data, in: 2019 International Conference on Computer, Control, Informatics and Its Applications: Emerging Trends in Big Data and Artificial Intelligence, IC3INA 2019. https://doi.org/10.1109/IC3INA48034.2019.8949568

Weise, D.R., Stephens, S.L., Fujioka, F.M., Moody, T.J., Benoit, J., 2010. Estimation of fire danger in Hawai'i using limited weather data and simulation. Pacific Sci. 64. https://doi.org/10.2984/64.2.199

Yang, X.S., 2009. Firefly algorithms for multimodal optimization, in: Lecture Notes in Computer Science (Including Subseries Lecture Notes in Artificial Intelligence and Lecture Notes in Bioinformatics). https://doi.org/10.1007/978-3-642-04944-6_14

Yelenik, S., Trauernicht, C., McDaniel, S., Wolkis, D., Chambers, T., 2024. Increasing wildfire incidence and the need for seed in Hawai'i. Nativ. Plants J. 25, 61–67.

Yin, J., He, B., Fan, C., Chen, R., Zhang, H., Zhang, Y., 2024. Drought-related wildfire accounts for one-third of the forest wildfires in subtropical China. Agric. For. Meteorol. 346. https://doi.org/10.1016/j.agrformet.2024.109893

Zhu, T.R., Litton, C.M., 2019. Modeling fuels and wildfire behavior in Hawaiian ecosystems 81.